ARTICLES
https://doi.org/10.1038/s41590-018-0290-0

nature immunology

Corrected: Publisher Correction

Uncoupling protein 2 reprograms the tumor microenvironment to support the anti-tumor immune cycle

Wan-Chen Cheng[1,2], Yao-Chen Tsui[1,2], Simone Ragusa[1,2,3], Viktor H. Koelzer[4], Marco Mina[5,6], Fabien Franco[1,2], Heinz Läubli[7], Benjamin Tschumi[1,2], Daniel Speiser[1,2], Pedro Romero[1,2], Alfred Zippelius[7], Tatiana V. Petrova[1,2,3], Kirsten Mertz[4], Giovanni Ciriello[5,6] and Ping-Chih Ho[1,2*]

Immune checkpoint blockade therapy has shifted the paradigm for cancer treatment. However, the majority of patients lack effective responses due to insufficient T cell infiltration in tumors. Here we show that expression of mitochondrial uncoupling protein 2 (UCP2) in tumor cells determines the immunostimulatory feature of the tumor microenvironment (TME) and is positively associated with prolonged survival. UCP2 reprograms the immune state of the TME by altering its cytokine milieu in an interferon regulatory factor 5-dependent manner. Consequently, UCP2 boosts the conventional type 1 dendritic cell- and CD8$^+$ T cell-dependent anti-tumor immune cycle and normalizes the tumor vasculature. Finally we show, using either a genetic or pharmacological approach, that induction of UCP2 sensitizes melanomas to programmed cell death protein-1 blockade treatment and elicits effective anti-tumor responses. Together, this study demonstrates that targeting the UCP2 pathway is a potent strategy for alleviating the immunosuppressive TME and overcoming the primary resistance of programmed cell death protein-1 blockade.

Immune checkpoint blockade (ICB) therapy elicits a marked clinical response in patients with different tumor types and changes the paradigm for cancer treatment[1–3]. However, the efficacy of ICB is hampered by a high rate of primary resistance[4,5]. Non-T cell-inflamed TME represents a major form of primary resistance[6–8]. Increased tumor infiltration of cDC1 (conventional type 1 dendritic cells), a subset of dendritic cells with superior cross-presentation capability, is a key event in guiding CD8$^+$ T cell infiltration in tumors[9,10]. However, oncogenic pathways, such as the active β-catenin signal and prostaglandin E2 (PGE2) production, attenuate cDC1 tumor infiltration and lead to T cell exclusion by suppressing cDC1-recruiting chemokine levels in tumors[9–11]. Thus, targeting deregulation of the β-catenin pathway and PGE2 signal axis has been suggested to break immunosuppressive TME in certain tumors having these immunosuppressive mechanisms. Unlike the targeting of oncogenic pathways, treatments using agonists of the stimulator of interferon genes (STING) and Toll-like receptor (TLR) pathways enhance CD8$^+$ T cell recruitment in tumors by activating antigen-presenting cells, especially cDC1[12,13]. However, systemic activation of antigen-presenting cells under treatments with STING and TLR agonists can disturb immune homeostasis and potentially exaggerate autoimmunity. These findings underscore the importance of alleviating the pathways that restrict cDC1 recruitment in tumors; however, other important issues remain, including how cDC1 and T cell tumor infiltration can be stimulated in tumors not harboring targetable oncogenic pathways and, precisely, how to induce T cell anti-tumor immunity without perturbing systemic immune homeostasis.

The mitochondrial protein UCP2 is ubiquitously expressed in multiple cell types and has a paradoxical role in tumorigenesis in a variety of tumor cells[14–18]. The effect of UCP2 in the generation of reactive oxygen species (ROS) in different stages of tumor progression has been suggested as the underlying mechanism for its paradoxical role in tumorigenesis and chemoresistance. However, some studies have reported that UCP2 expression does not affect ROS production, highlighting that UCP2 might act as a modulator to fine-tune metabolic preferences of cancer cells[17,19,20]. In addition to intrinsic regulations for cancer cell growth and chemoresistance, it remains unknown whether the expression of UCP2 in tumor cells affects their ability to evade immunosurveillance.

Here we integrate analyses of human melanoma patients from The Cancer Genome Atlas (TCGA) cohort and mouse melanoma models, and find that increased UCP2 expression in melanoma cells reprograms the TME into T cell-inflamed tumors. Our data indicate that UCP2 induction in melanoma cells blocks the immunosuppressive feature of the TME by shifting the cytokine milieu, leading to engagement of the cDC1-CD8$^+$ T cell anti-tumor immune cycle. Furthermore, we provide proof-of-concept evidence that inducing UCP2 expression with genetic and pharmacological interventions can suppress tumor progression and sensitize programmed cell death protein-1 (PD-1) blockade-resistant melanomas to anti-PD-1 antibody treatment.

Results

UCP2 expression is associated with elevated T cell anti-tumor immunity. To elucidate potential targets that stimulate T cell anti-tumor immune responses in the TME, we first characterized melanoma patients from TCGA with either high or low T cell anti-tumor immune responses, by determining expression signature scores for seven gene sets that have been reported as indicators of increased

[1]Department of Fundamental Oncology, University of Lausanne, Lausanne, Switzerland. [2]Ludwig Cancer Research, University of Lausanne, Epalinges, Switzerland. [3]Division of Experimental Pathology, CHUV, Lausanne, Switzerland. [4]Institute of Pathology, Cantonal Hospital Baselland, Liestal, Switzerland. [5]Department of Computational Biology, University of Lausanne, Lausanne, Switzerland. [6]Swiss Institute of Bioinformatics, Lausanne, Switzerland. [7]Department of Biomedicine, University Hospital Basel, Basel, Switzerland. *e-mail: ping-chih.ho@unil.ch

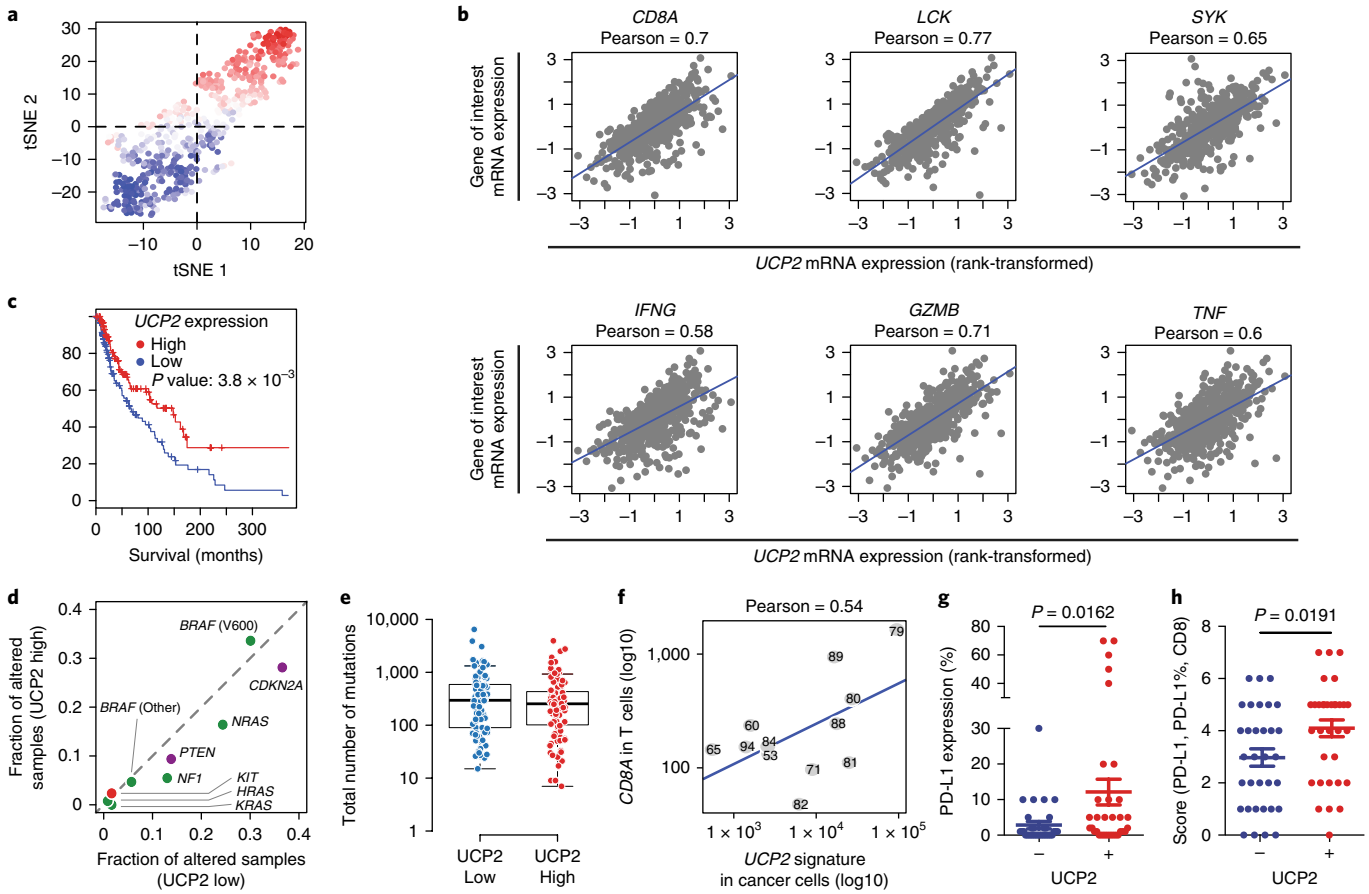

Fig. 1 | UCP2 expression is associated with elevated T cell infiltration and prolonged survival rates. a, T-distributed stochastic neighbor-embedding (tSNE) plot of melanoma patients according to combined T cell anti-tumor response signature scores. **b**, Pearson correlation of UCP2 expression with *CD8A*, IFNG, GZMB, TNF, LCK and *SYK*. **c**, Kaplan–Meier survival curves of melanoma patients with high and low UCP2 expression (top and bottom 25%). $P = 3.8 \times 10^{-3}$ (Mantel–Cox test). **d**, Distribution plot of major melanoma driver mutations in melanoma patients with either low or high UCP2 expression. **e**, Total number of mutations in $UCP2^{lo}$ and $UCP2^{hi}$ melanoma patients (**a**–**e**, $n = 472$ biologically independent melanoma tumor samples from TCGA cohort). The box extends between 25 and 75%, and the whisker extends up to the 75% + 1.5 inter-quantile range and down to the 25%. UCP2 low: 0% (15), 25% (90), 50% (296), 75% (590), 100% (6,470); UCP2 high: 0% (7), 25% (101.5), 50% (254), 75% (432), 100% (3,942). **f**, Association between the expression of UCP2 signature in melanoma cells and CD8A gene expression in T cells (Pearson correlation = 0.54, $P = 0.034$, $n = 12$). Data from Tirosh et al. single-cell RNA-seq dataset[27]. Each dot represents one patient. **g**, **h**, Quantitative results of immunohistochemistry staining against UCP2, CD8A and programmed death-ligand 1 (PD-L1) in 66 melanoma patients. PD-L1 expression percentage in melanoma cells ($P = 0.0162$) (**g**) and the combined scores of CD8A intensity and PD-L1 expression percentage and intensity ($P = 0.0191$) (**h**) in sections with or without UCP2 expression in melanoma cells. Each symbol represents an individual patient (**g**, **h**, both groups $n = 33$). Data are mean ± s.e.m. and were analyzed by unpaired, two-tailed Student's *t*-test. Correlation was assessed using the Pearson correlation coefficient.

T cell infiltration and anti-tumor response (Supplementary Table 1)[9,21–23]. Multidimensional scaling of these patients, based on their transcriptional scores, identified two groups with either high or low combined expression scores, suggesting that we could classify patients into those with either high or low T cell anti-tumor responses (Fig. 1a). Differentially expressed genes between the two groups were highly enriched for those controlling defense responses, inflammatory responses and T cell activation (Supplementary Fig. 1a). Among the top gene hits upregulated in patients with high T cell anti-tumor responses, we identified that UCP2 was the top-ranked metabolic enzyme. Further analyses revealed a positive correlation between *UCP2* messenger RNA (mRNA) and individual gene transcripts related to T cell infiltration and anti-tumor immunity, including *CD8A*, *IFNG*, *GZMB*, *TNF*, *LCK* and *SYK* (Fig. 1b), and patients expressing higher *UCP2* messenger RNA (mRNA) exhibited prolonged survival rates (Fig. 1c). Of note, the expression of other members of the UCP family did not display a strong association with gene transcripts related to T cell anti-tumor responses (Supplementary Fig. 1b), suggesting that UCP2 expression associated with elevated T cell anti-tumor responses in tumors is probably not a result of mitochondrial uncoupling, a general biological function of the UCP protein family. Moreover, UCP2 expression patterns in melanomas were independent of classical melanoma driver mutations (Fig. 1d), suggesting that UCP2 expression is not controlled by these classic oncogenic pathways in this tumor type. Since high somatic mutation rate in tumors has been suggested as increasing the frequency of neoantigen formation, leading to effective tumor rejection[24–26], we next determined whether mutation numbers were increased in melanoma patients with high UCP2 expression. Our results showed that melanoma patients with different UCP2 expression levels have similar numbers of mutations (Fig. 1e), indicating that increased T cell anti-tumor immune responses in patients with high UCP2 expression do not result from increased neoantigen burden.

By analyzing UCP2 expression in different cell types in human melanomas from a published single-cell RNA sequencing (scRNA-seq) dataset[27], we found that T and B cells express the highest level of UCP2 (Supplementary Fig. 2a). Therefore, UCP2 expression in

T cells could be a confounding factor leading to positive correlation between UCP2 expression and T cell anti-tumor signature in our analysis. To further examine whether UCP2 expression in melanoma cells is associated with stronger T cell anti-tumor responses, we first determined the correlation of *UCP2* mRNA expression in melanoma cells and *CD8A* mRNA abundance in tumor-infiltrating T lymphocytes. To acquire a more reliable readout indicating UCP2 expression in malignant cells, we defined a 'UCP2 signature' comprising genes that were co-expressed with UCP2 specifically in malignant melanoma cells, by cross-analyzing transcriptomes of $UCP2^{hi}$ and $UCP2^{lo}$ patients in CGA cohort and transcriptome of melanoma cells in the scRNA-seq dataset (Supplementary Fig. 2b,c and Supplementary Table 2). We found that expression of the UCP2 gene signature in melanoma cells positively correlated with the abundance of *CD8A* mRNA in tumor-infiltrating lymphocytes (Fig. 1f). In addition, we collected a validation cohort of melanoma patients and conducted immunohistochemical staining for UCP2 and CD8α, and PD-L1 in melanoma sections. We found that those sections with melanoma cells expressing UCP2 had higher frequencies of PD-L1 expression and exhibited higher T cell anti-tumor immune scores, calculated based on the combined scores of CD8α and PD-L1 staining intensity and percentage in melanoma cells (Fig. 1g,h). Of note, the frequency of PD-L1 expression and T cell anti-tumor immune scores were correlated with the level of UCP2 expression in melanoma cells (Supplementary Fig. 3a–c). In support of the findings from TCGA analysis, our results showed that UCP2 expression in melanoma cells was not linked with disease stage, age, gender or driver mutations in this validation patient cohort (Supplementary Table 3).

UCP2 expression is associated with an anti-tumor immune state of the TME. We next assessed the transcriptomes of TCGA melanoma patients with varying UCP2 expression and found that expression levels resulted in dramatic differences. We analyzed the top 500 differentially expressed genes in $UCP2^{hi}$ versus $UCP2^{lo}$ patients (adjusted $P < 3\times10^{-29}$) (Supplementary Table 4), and found that UCP2 mRNA was positively associated with genes controlling IFN-γ signaling and leukocyte activation and migration (Fig. 2a,b). Among those genes, we found that *UCP2* mRNA is strongly associated with gene transcripts that control migration of dendritic cells and T cell recruitment, including *CCL4*, *CCL5*, *CXCR3*, *CXCL9* and *CXCL10* (Fig. 2c). The strong positive association between UCP2 transcript and chemokines controlling migration of dendritic cells and T cells suggests that increased UCP2 expression in melanoma cells supports the anti-tumor immune cycle by producing immune-stimulatory chemokines in the TME. Previous studies have indicated that cDC1, which are dependent on basic leucine zipper transcriptional factor ATF-like 3 (BATF3) for development and express CD141 in humans and CD103 in mice as lineage markers, are crucial for priming $CD8^+$ T cells against tumor antigens and attracting tumor-specific $CD8^+$ T cells through the production of CXCL10[12,28–30]. CCL4 and CCL5 have been shown to support the migration of cDC1 into tumors through stimulation of CCR5 expressed in cDC1[9,10,29]. In support of this, we found that *UCP2* mRNA expression and cDC1 tumor infiltration, computationally predicted based on the expression levels of a core gene set of cDC1 (defined as BATF3-DC signature score)[29], were highly associated in melanoma patients from TCGA (Fig. 2d). Moreover, we observed that melanoma cells expressing UCP2 had higher frequencies of cDC1 in tumors as indicated by XCR1 staining (Fig. 2e). Furthermore, we found that UCP2 mRNA was strongly associated with T cell infiltration signature in multiple tumor types (Fig. 2f). Together, our results suggest that UCP2 expression in tumor cells, especially melanoma cells, results in an immunostimulatory chemokine profile and infiltration of $CD8^+$ T cells and cDC1 in the TME.

UCP2 induction in melanoma cells suppresses tumor progression. To further investigate whether UCP2 expression in melanoma cells stimulates anti-tumor T cell responses, we established a doxycycline (Dox)-inducible B16-OVA melanoma cell line, which stably expresses ovalbumin and inducibly expresses either flag-tagged UCP2 (3F-UCP2) or flag tag (3F) following Dox treatment. We engrafted 3F and 3F-UCP2 B16-OVA into the left and right flank of WT mice, respectively. The mice were then treated with control vehicle or Dox-containing water at day 7 post-tumor engraftment to induce either flag tag or 3F-UCP2 expression in melanoma cells (Fig. 3a). We found that flag tag and 3F-UCP2 melanomas displayed similar growth rates under control vehicle treatment. However, Dox treatment drastically suppressed the growth of 3F-UCP2 melanomas, but not flag tag melanomas (Fig. 3b,c). Of note, overexpression of UCP2 in the YUMM1.7 melanoma cell line, which harbors a $Braf^{V600E}$ mutation and PTEN deletion[31], using the same approach also suppressed in vivo tumor growth (data not shown). We next investigated whether UCP2 induction in melanoma cells modulates immune infiltrates in the TME. We found that UCP2 overexpression promoted tumor infiltration of $CD8^+$ T cells and NK cells (Fig. 3d,e and Supplementary Fig. 4a,b), but had no effect on $CD4^+$ T cells, regulatory T cells (Tregs) or B cells (Supplementary Fig. 5c–f). Despite increasing numbers of tumor-infiltrating $CD8^+$ T cells (TILs) in tumors, UCP2 overexpression in melanoma cells did not enhance the functional capacity of $CD8^+$ TILs, including proinflammatory cytokine IFN-γ and tumor necrosis factor production (Supplementary Fig. 4g,h). Of note, UCP2-overexpressing B16-OVA cells displayed similar levels of major histocompatibility complex I (MHCI) and antigen-presentation capability, as measured by in vitro coupling assay, compared to control cells (Supplementary Fig. 4i,j). Although UCP2 overexpression slightly enhanced PD-L1 expression in B16 melanoma cells (Supplementary Fig. 4k), it did not affect the cytotoxicity of $CD8^+$ T cells in the in vitro killing assay (Supplementary Fig. 4l). Together, our results suggest that UCP2 induction does not promote antigen presentation in melanoma cells.

UCP2 has been shown to affect tumor progression and chemoresistance by mitigating ROS production through its uncoupling effect[14,16,32]. However, in agreement with other works[17,19], we found that UCP2 induction did not affect total intracellular and mitochondrial ROS in B16 melanoma cells (Supplementary Fig. 5a,b), suggesting that UCP2 induction-mediated tumor regression does not result from changes in ROS-mediated signaling cascades. UCP2 has also been shown to promote metabolic dependence on oxidative phosphorylation of melanoma cells through downregulation of hypoxia-inducible factor 1 (HIF-1) and suppression of the mTOR pathway[17]. Thus, we postulated that UCP2 induction in melanoma cells might restrict aerobic glycolysis and spare glucose to facilitate the metabolic fitness of $CD8^+$ TILs. To test this, we generated a Dox dual-inducible B16-OVA cell line to overexpress UCP2 and a myc-tagged stabilized mutant of HIF-1α[33]. We confirmed that overexpression of the stabilized mutant of HIF-1α prevented UCP2-mediated mTOR pathway suppression (based on phosphorylation levels of S6 and Akt) (Supplementary Fig. 5c) and sustained glucose consumption (data not shown). However, UCP2 overexpression remained effective in inhibiting tumor progression when melanoma cells simultaneously expressed the stabilized mutant of HIF-1α (Supplementary Fig. 5d,e), ruling out the possibility that UCP2-stimulated T cell anti-tumor immunity is a result of metabolic reprogramming of melanoma cells. Together, these data indicate that UCP2 induction in melanoma cells stimulates $CD8^+$ T cell-mediated anti-tumor responses through the engagement of undefined mechanisms.

UCP2 overexpression evokes $CD8^+$ T cell-dependent anti-tumor immune responses. We next sought to investigate whether UCP2 overexpression affects the spatial distribution of

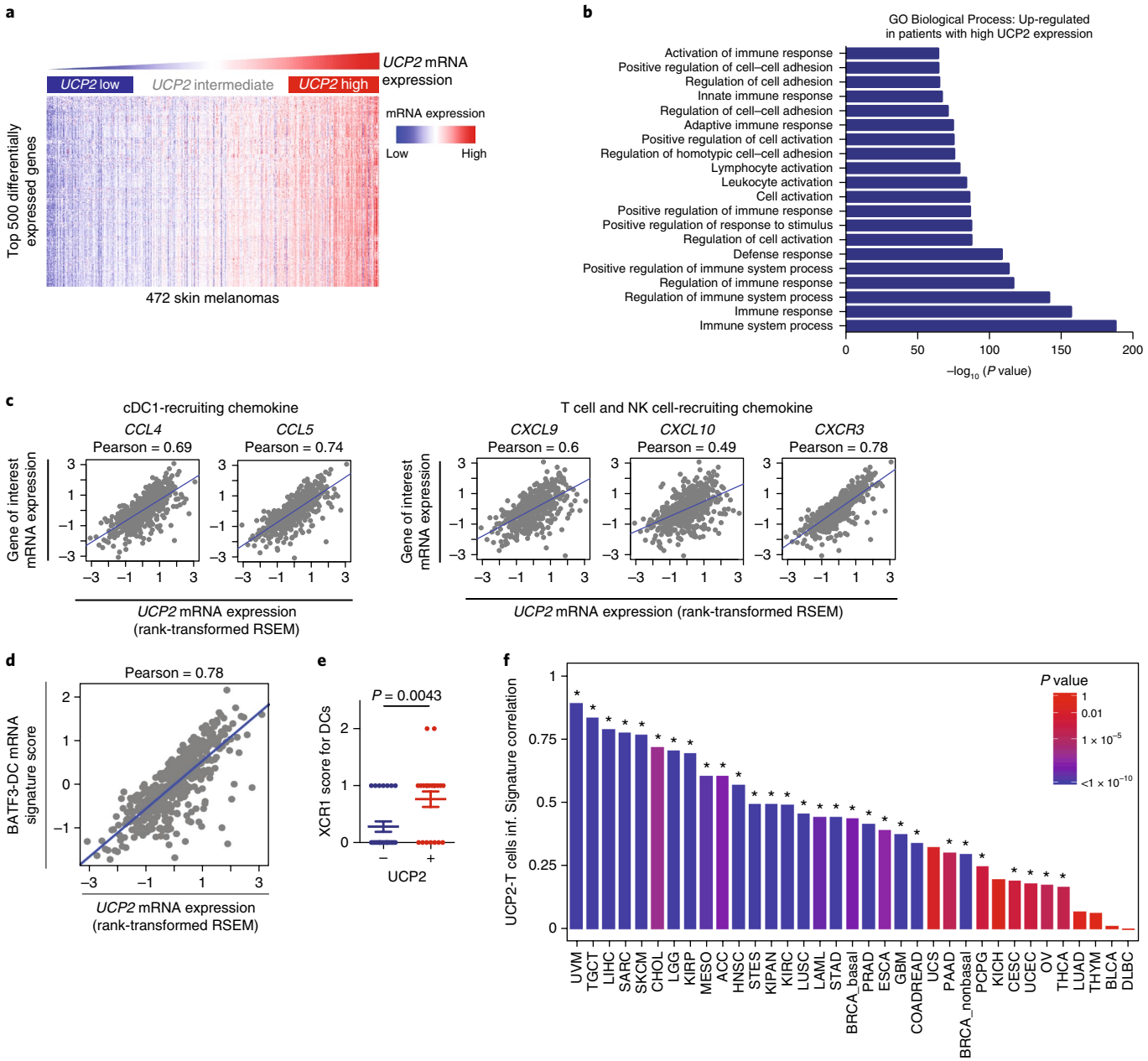

Fig. 2 | UCP2 expression is associated with anti-tumor immune states and cDC1 and CD8⁺ T cell infiltration in tumors. a, Expression of top 500 genes upregulated in melanoma patients with high UCP2 expression. **b**, Gene ontology term enrichment analysis for top 20 biological process controlled by differentially expressed genes among patients with high UCP2 expression. **c**, Pearson correlation of UCP2 gene expression with indicated transcripts of cDC1- and T cell-recruiting chemokines. RSEM, relative s.e.m. **d**, Pearson correlation of UCP2 expression with BATF3-DC signature score in melanoma patients. **e**, Quantitative results of immunohistochemistry staining against XCR1 in tumor-infiltrating dendritic cells (DCs) of 46 melanoma patient samples (UCP2⁻, $n=25$; UCP2⁺, $n=21$). **f**, Correlation plot of *UCP2* expression and T cell infiltration gene signature in pan-tumor types (**a**–**d**,**f**, $n=472$, biologically independent melanoma tumor samples from TCGA cohort). Correlation and two-tailed *P* values were assessed using the Pearson correlation coefficient and upaired *t*-test. **e**, Data are mean ± s.e.m. and were analyzed by unpaired, two-tailed Student's *t*-test. *$P \leq 0.01$.

CD8⁺ TILs and tumor vasculature. We assessed CD8⁺ T cell infiltration, vascular morphology and mural cell coverage, essential for vascular integrity and maturity, by staining for CD8α, SMA (smooth muscle B-actin, a marker of tumor pericytes and vascular smooth muscle cells) and vascular endothelial cadherin (VE-cadherin, a marker of endothelial cells). UCP2 overexpression enhanced CD8⁺ TIL infiltration in YUMM1.7-OVA melanomas and strongly increased both the proportion of mural cell-covered tumor vessels and individual vessel size (Fig. 3f–i), suggesting that UCP2 induction normalizes tumor microvasculature. Similar to YUMM1.7 melanoma, UCP2 overexpression increased CD8⁺ TIL infiltration in the margins, and especially the core, of B16-OVA melanomas (Supplementary Fig. 6a). Vessel size, mural cell coverage and the expression of lymphocyte adhesion receptor VCAM-1 on endothelial cells were increased in the core of UCP2-overexpressing tumors (Supplementary Fig. 6b–d). Given that enhanced T cell immune responses can also facilitate tumor vessel normalization through hitherto undefined mechanisms[34], we next examined whether T cells are required for UCP2 overexpression-induced vessel normalization using either *Rag1*$^{-/-}$

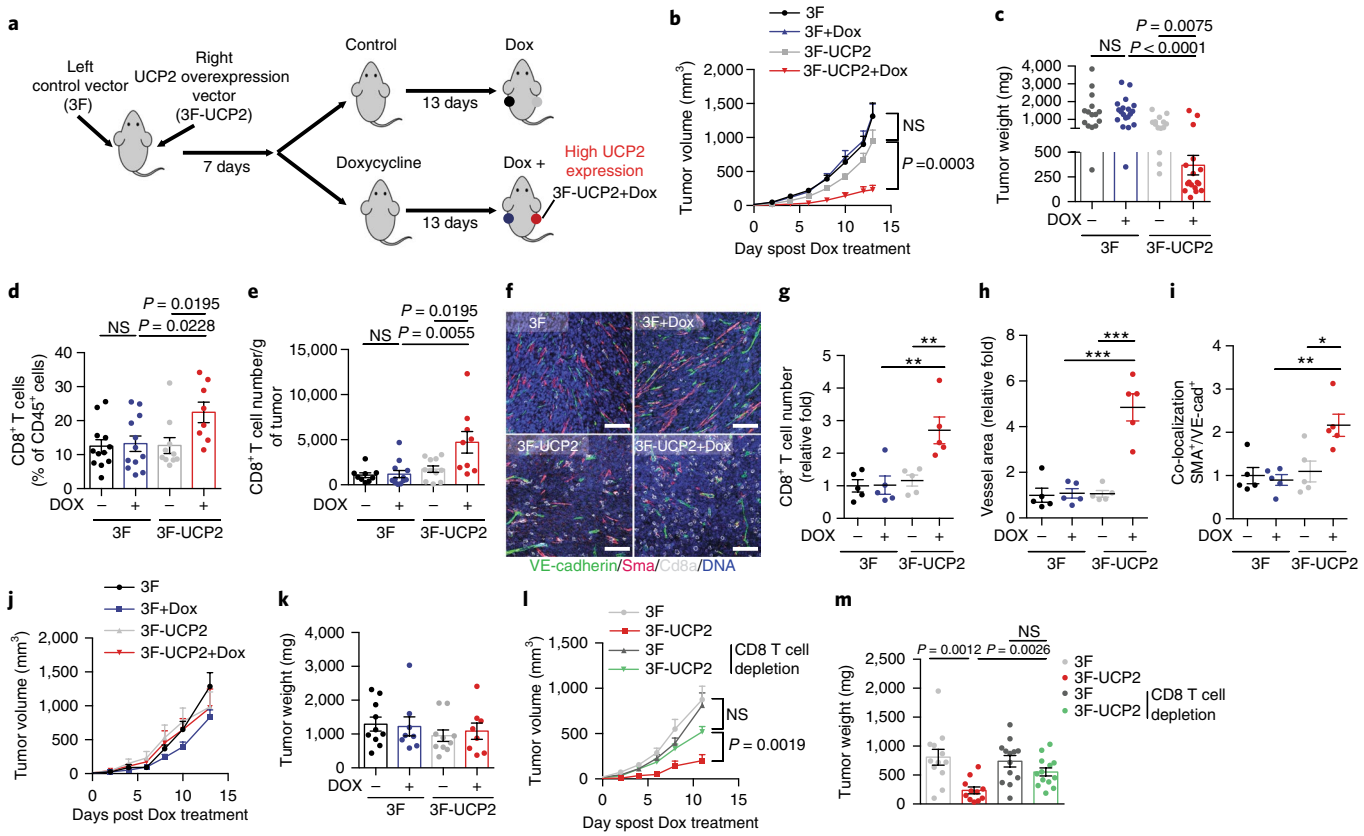

Fig. 3 | UCP2 overexpression in melanoma cells induces anti-tumor responses and normalizes tumor vasculature. a, Experimental scheme. **b**,**c**, Tumor growth (**b**) and tumor weight (**c**) of indicated melanomas from control or Dox-treated co-engrafted mice (3F, $n=15$; 3F + Dox, $n=19$; 3F-UCP2, $n=14$; 3F-UCP2 + Dox, $n=17$). **d**,**e**, Percentage (**d**) and absolute number of CD8$^+$ T cells per gram tumor (**e**) from indicated tumor-bearing mice (3F, $n=9$; 3F + Dox, $n=12$; 3F-UCP2, $n=11$; 3F-UCP2 + Dox, $n=9$). **f**, Representative images of immunofluorescent staining for indicated proteins and DNA in YUMM1.7-OVA melanomas. Scale bar, 100 μm. **g**–**i**, Quantification of the data shown in **f** ($n=5$ in each group). **g**, Relative number of TILs (analysis of variance (ANOVA) $P=0.0019$). **h**, relative single-tumor vessel area (ANOVA $P<0.0001$). **i**, Relative mural smooth muscle β-actin (a marker of tumor pericytes and vascular smooth muscle cells) (SMA)$^+$ cell coverage of vascular endothelial cadherin$^+$ blood vessels (ANOVA $P=0.0019$). **j**,**k**, Tumor growth (**j**) and tumor weight (**k**) of indicated melanomas from co-engrafted *Rag1*$^{-/-}$ mice treated with indicated treatments. **l**,**m**, Tumor growth (**l**) and tumor weight (**m**) of indicated melanomas from mice treated with Dox with or without anti-CD8 antibody injection (Dox-only groups: 3F, $n=12$; 3F-UCP2, $n=11$; Dox plus CD8 depletion groups: 3F, $n=13$; 3F-UCP2, $n=13$). Data are mean ± s.e.m. and were analyzed by two-tailed, unpaired Student's *t*-test (**b**–**e**,**j**–**m**) or one-way ANOVA with Tukey's multiple comparison test (**g**–**i**). Data are cumulative results from at least three independent experiments (**b**–**e**,**j**–**m**), two independent experiments (**g**–**i**) or representative images of two independent experiments (**f**). *$P\leq0.05$, **$P\leq0.01$, ***$P\leq0.001$. NS, not significant. Each symbol represents an individual mouse.

or CD8$^+$ T cell-depleted mice as recipient. We found that UCP2 overexpression in melanoma cells was sufficient to increase mural vascular coverage, but not vessel size, in those immunocompromised recipients (Supplementary Fig. 6e–h). Together, these results demonstrate that UCP2 induction in melanomas facilitates recruitment of CD8$^+$ T cells into the tumor core and normalizes tumor vessels, which are critical features of enhanced anti-tumor immunity and sensitivity to PD-1 blockade treatment[35].

To better understand whether T cell-mediated immune responses are needed for UCP2-induced tumor suppression, we performed the same engraftment using *Rag1*$^{-/-}$ mice as recipient. Our results showed that inducing UCP2 overexpression in melanoma cells failed to suppress tumor progression in *Rag1*$^{-/-}$ mice, indicating that T cell- and/or B cell-mediated immunity is required to restrict tumor progression following UCP2 overexpression (Fig. 3j,k). We further found that UCP2-induced anti-tumor responses were CD8$^+$ T cell-dependent, since CD8$^+$ T cell depletion abrogated anti-tumor responses induced by UCP2 overexpression (Fig. 3l,m). Thus, we conclude that UCP2 expression in melanoma cells impedes tumor growth by facilitating CD8$^+$ TIL recruitment and mounts an effective response against tumors.

UCP2 induction supports cDC1-dependent anti-tumor response. To further understand whether UCP2 induction in melanoma cells reprograms the cytokine milieu in tumors as we observed in the human melanoma TCGA cohort, we determined the cytokine profiles of tumors overexpressing UCP2 or control vector from Dox-treated co-engrafted mice. Consistent with TCGA analysis, our results showed that UCP2 induction promoted the production of cytokines and molecules known to support anti-tumor immunity—CCL4, CCL5, CXCL9, CXCL10, IFN-γ, IL-28 and ICAM-1 (Fig. 4a,b). In contrast, UCP2 overexpression suppressed the expression of pro-tumorigenic factors IL-10 and M-CSF, and angiogenesis factors VEGF and angiopoietin-2. In agreement with our observations from TCGA, we found that UCP2 overexpression increased cDC1 infiltration in the co-engraftment model (Fig. 4c). Next, we sought to examine whether cDC1 are required for UCP2-mediated anti-tumor responses. We performed the same tumor co-engraftment experiment in WT and BATF3-knockout (*Batf3*$^{-/-}$) mice, which failed to develop cDC1[28]. Our results showed that UCP2 overexpression remained effective at suppressing tumor growth in WT mice, but not in *Batf3*$^{-/-}$mice (Fig. 4d,e), and failed to facilitate CD8$^+$ TIL recruitment in *Batf3*$^{-/-}$ mice (Fig. 4f). Collectively, our data indicate

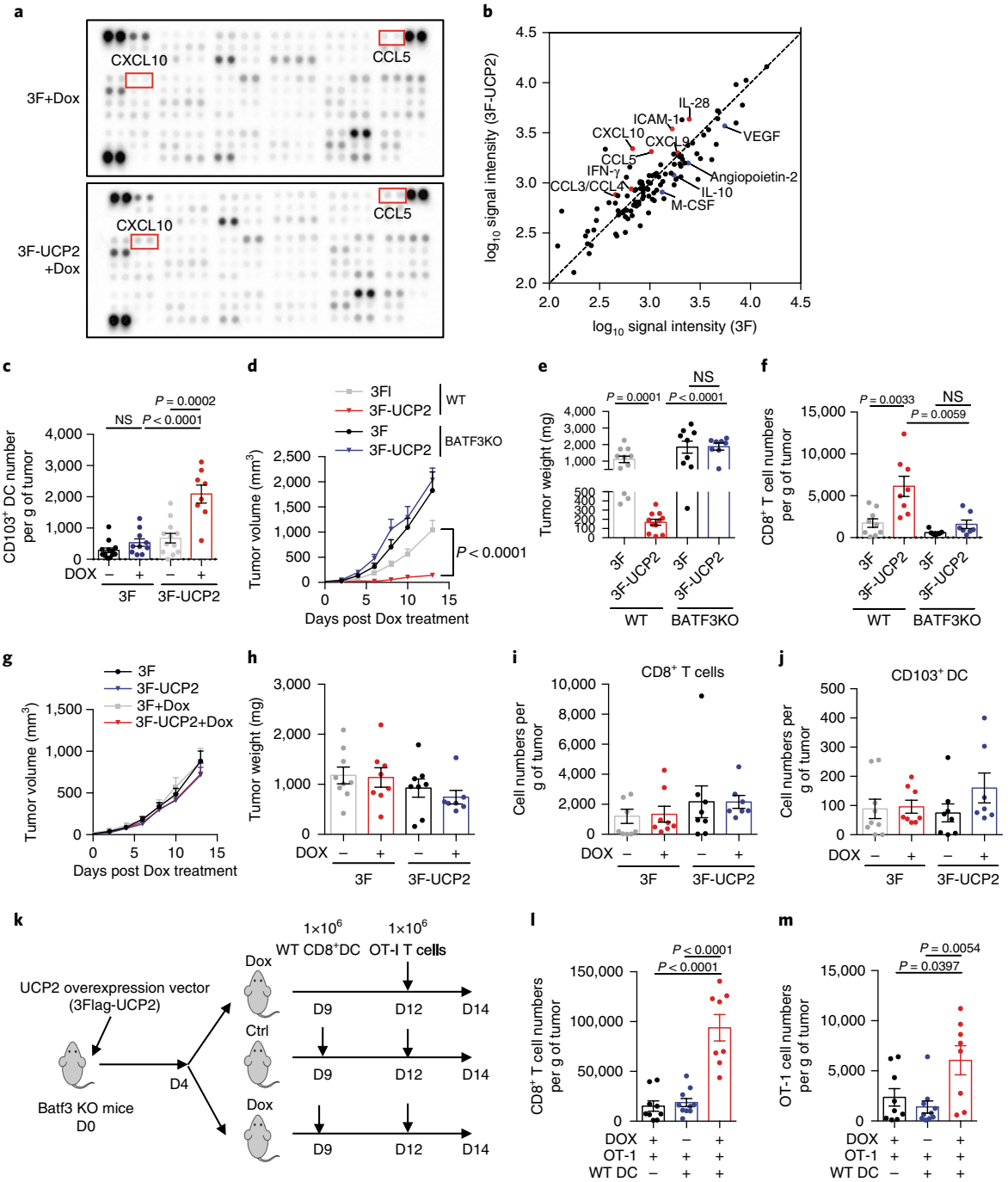

Fig. 4 | UCP2-induced anti-tumor responses are associated with the immune state and are dependent on CD103⁺ dendritic cells. a,**b**, Representative images (**a**) and expression patterns of chemokines (**b**) from proteome array analysis of control (3F + Dox) and UCP2-overexpressing (3F-UCP2 + Dox) tumors. **c**, Absolute number of CD103⁺ dendritic cells (DCs) per gram tumor of 3F and 3F-UCP2 B16-OVA melanomas from co-engrafted mice treated with or without Dox (3F, $n=13$; 3F + Dox, $n=10$; 3F-UCP2, $n=12$; 3F-UCP2 + Dox, $n=8$). **d**–**f**, Tumor growth (**d**), tumor weight (**e**) and absolute number of CD8⁺ T cells per gram tumor (**d**,**e**, WT groups: 3F, $n=11$; 3F-UCP2, $n=11$; *Batf3*$^{-/-}$ groups: 3F, $n=9$, 3F-UCP2, $n=8$) (**f**, WT groups: 3F, $n=9$; 3F-UCP2, $n=8$; *Batf3*$^{-/-}$ groups: 3F, $n=7$, 3F-UCP2, $n=7$) of 3F- and 3F-UCP2 B16-OVA melanomas from co-engrafted C57BL/6 mice (WT) or *Batf3*$^{-/-}$ mice (BTAF3 KO) treated with Dox. **g**–**j**, Tumor growth (**g**), tumor weight (**h**), absolute number of CD8⁺ T cells per gram tumor (**i**) and absolute number of CD103⁺ DCs per gram tumor (**j**) of 3F and 3F-UCP2 B16-OVA melanomas from co-engrafted *Ccr5*$^{-/-}$ mice treated with or without Dox (3F, $n=9$; 3F + Dox, $n=8$; 3F-UCP2, $n=8$; 3F-UCP2 + Dox, $n=7$). **k**, Experimental scheme of in vivo CD8⁺ DC and OT-I T cell transfer experiment. **l**,**m**, Absolute number of polyclonal CD8⁺ T cells per gram tumor (**l**) and OT-I T cells per gram tumor (**m**) from indicated groups of mice (Dox⁺/OT-I⁺ group, $n=9$; Dox⁻/OT-I⁺/WT DC⁺ group, $n=10$; Dox⁺/OT-I⁺/WT DC⁺ group, $n=8$). Data are mean ± s.e.m. and were analyzed by unpaired, two-tailed Student's *t*-test. Data are cumulative results from at least three independent experiments (**c**–**j**,**l**,**m**) or representative images of two independent experiments (**a**,**b**). NS, not significant. Each symbol represents an individual mouse.

that elevated UCP2 expression in melanoma cells can boost the production of anti-tumorigenic chemokines and molecules to facilitate cDC1 infiltration and anti-tumor immune responses. Given that the expression of CCR5 in cDC1 plays a critical role in modulating tumor infiltration of cDC1[29], and that CCR5-deficient mice (*Ccr5*$^{-/-}$) have normal T cell priming[36], we then examined UCP2-mediated

anti-tumor responses in *Ccr5*$^{-/-}$ mice. We found that UCP2 induction failed to suppress tumor progression and promote recruitment of CD8$^+$ TIL and cDC1 in these mice (Fig. 4g–j). Furthermore, in *Batf3*$^{-/-}$ mice we examined CD8$^+$ TIL infiltration reconstituting with cDC1 and activated OT-I cells (Fig. 4k). We observed similar levels of tumor infiltration of polyclonal CD8$^+$ T cells and OT-I cells in DOX-treated *Batf3*$^{-/-}$ mice reconstituting with OT-I alone, and in control vehicle-treated *Batf3*$^{-/-}$ mice reconstituting with OT-I and cDC1 cells. In contrast, UCP2 induction enhanced tumor infiltration of polyclonal CD8$^+$ T cells and OT-I cells in *Batf3*$^{-/-}$ mice reconstituting with both OT-I and cDC1 cells (Fig. 4l,m), suggesting that UCP2-induced CD8$^+$ TIL infiltration is cDC1 dependent. Taken together, these results reveal that UCP2 expression in melanoma cells can reprogram the TME into an immune-stimulatory microenvironment that mounts a cDC1-CD8$^+$ T cell-dependent anti-tumor response.

The IRF5–CXCL10 axis supports engagement of the anti-tumor immune cycle. To understand how UCP2 induction in melanoma cells affects chemokine profiles in the TME, we next examined changes in the transcriptome of melanoma cells following UCP2 overexpression. UCP2 induction promoted expression of *CXCL10*, but not *CCL5* and *CCL4* (Fig. 5a), suggesting that UCP2 overexpression in melanoma cells may enhance CCL5 and CCL4 levels in the TME through its production by other cell types. Given that CXCL10 attracts both CD8$^+$ T and NK cells, which have been reported to be the main producers of CCL5 in melanomas[10], we thus speculated that UCP2-overexpressing melanomas facilitate a low level of CD8$^+$ T cell recruitment through upregulation of CXCL10 production from melanoma cells. This low-grade increase in CD8$^+$ TILs may lead to upregulation of CCL5 in tumors. The increasing involvement of CCL5 supports cDC1 tumor infiltration, which further enhances CD8$^+$ TIL recruitment through CXCL10 production. In support of this postulate, we found that depletion of CD8$^+$ T cells abrogated the induction of both CCL5 (Fig. 5b) and CXCL10 (Fig. 5c), and impaired cDC1 tumor infiltration in UCP2-overexpressing melanomas (Fig. 5d). Thus, our data suggest that CD8$^+$ T cells are the major producers of CCL5 following UCP2 induction, and that the presence of CD8$^+$ T cells is critical in maximizing cDC1 infiltration. Interestingly, we found that UCP2 induction stimulated expression of interferon regulatory factor 5 (IRF5) (Fig. 5e), a transcription factor that stimulates CXCL10 expression[37,38] and has been suggested to affect immune responses in melanoma patients[39]. Furthermore, the expression of UCP2 and IRF5 was also highly associated in patients in TCGA cohort (Fig. 5f) and expression of the UCP2 gene signature is also associated with *IRF5* expression in melanoma cells, based on scRNA-seq analysis (Fig. 5g). In addition, melanoma cells expressing UCP2 showed a higher frequency of IRF5 expression in our validation cohort of melanoma patients (Fig. 5h). Thus, we speculated that UCP2 overexpression in melanoma cells could promote CXCL10 production through IRF5-dependent transcriptional regulation. In support of this, we found that silencing IRF5 abrogated UCP2-induced CXCL10 production (data not shown). To further examine whether IRF5-mediated CXCL10 production in melanoma cells contributes to UCP2-induced cDC1-CD8$^+$ T cell anti-tumor immune cycle engagement, we generated 3F-UCP2 B16-OVA cells stably expressing short-hairpin RNA interference targeting either IRF5 or CXCL10. Our results showed that UCP2 overexpression failed to suppress tumor growth (Fig. 5i,j) and was incapable of stimulating cDC1 and CD8$^+$ T cell recruitment (Fig. 5k,l) in either IRF5- or CXCL10-deficient B16-OVA melanomas. We next evaluated the relationships between the expression of UCP2 and IRF5 in melanoma cells and cDC1 infiltration (as measured by XCR1 staining in dendritic cells) in our validation melanoma patient cohort. The results showed that the majority of tumor sections with UCP2 and IRF5 expression in melanoma cells contained XCR1$^+$ DCs. In contrast, there were no XCR1$^+$ dendritic cells in most sections in which melanoma cells expressed negligible UCP2 and IRF5 levels (Fig. 5m). Taken together, these results demonstrate that UCP2 overexpression promotes engagement and amplification of the cDC1-CD8$^+$ T cell anti-tumor immune cycle by stimulating IRF5-dependent CXCL10 production.

Melanoma UCP2 expression is independent of both β-catenin pathway and PGE2 production. Active β-catenin signaling in melanoma cells has been reported to block cDC1 infiltration via an ATF3-dependent mechanism[9]. Through analysis of TCGA melanoma patients, we found that UCP2 expression inversely, but moderately, correlated with *CTNNB1* score (based on the expression levels of six β-catenin signaling target genes)[9] (Fig. 6a). However, our results showed that UCP2 overexpression neither suppressed the expression of β-catenin signaling target genes nor inhibited ATF3 expression in B16 melanoma cells (Fig. 6b,c). In addition to the β-catenin signaling pathway, PGE2 production in melanoma cells has also been reported to support immune evasion by impairing cDC1 tumor infiltration[10,40]. However, the expression of UCP2 mRNA was not associated with reduction in gene transcripts of *PTGS1* and *PTGS2* in TCGA cohort (Fig. 6d,e). Together, our data suggest that suppression of UCP2-induced cDC1 tumor infiltration may be controlled by a mechanism that acts in parallel with β-catenin signaling and PGE2 production to block cDC1 tumor infiltration.

Induction of UCP2 expression sensitizes melanomas to PD-1 blockade treatment. Next, we postulated that UCP2 induction might ameliorate primary resistance to anti-PD-1 treatment in melanomas by inflaming non-T cell inflamed tumor. To investigate this, we engrafted mice with 3F-UCP2 B16-OVA and then treated tumor-bearing mice with either control vehicle or Dox with or without anti-PD-1 monoclonal antibody. As reported previously, B16-OVA melanoma cells were resistant to anti-PD-1 monoclonal antibody treatment[41]. Strikingly, UCP2 induction sensitized B16-OVA melanomas to anti-PD-1 therapy and prolonged the survival of tumor-bearing mice (Fig. 7a,b), suggesting that UCP2 induction can overcome primary resistance to PD-1 blockade in melanomas. Since peroxisome proliferator-activator receptor agonists promote UCP2 expression in adipocytes and hepatocytes[42,43], we suspected that these agonists might represent candidate molecules for induction of UCP2 expression in melanoma cells. Indeed, rosiglitazone, a drug approved by the Food & Drug Administration for diabetes treatment, promoted UCP2 expression in B16-OVA and YUMM1.7-OVA cells (Fig. 7c; data not shown). We therefore examined whether rosiglitazone could sensitize melanomas to anti-PD-1 treatment similar to the genetic induction of UCP2. Indeed, we found that rosiglitazone sensitized B16-OVA melanomas to PD-1 blockade and prolonged the survival of tumor-bearing mice (Fig. 7d,e). In contrast, rosiglitazone failed to sensitize B16-OVA melanomas to anti-PD-1 treatment in *Batf3*$^{-/-}$ mice (Fig. 7f), indicating that the combination treatment of rosiglitazone and anti-PD-1 monoclonal antibody used to overcome the primary resistance of PD-1 blockade is cDC1 dependent. To examine whether rosiglitazone enhances the therapeutic responses of anti-PD-1 antibody treatment in a UCP2-dependent manner, we engineered a UCP2-deficient melanoma cell line using CRSIPR-mediated genome editing (Fig. 7g). Our results showed that the combination treatment failed to suppress UCP2-deficient melanoma growth, and to prolong the survival of tumor-bearing mice (Fig. 7h,i), suggesting that UCP2 expression in melanoma cells is critical for rosiglitazone-mediated sensitization to PD-1 blockade. We further utilized a non-T cell-inflamed Braf/Pten melanoma model, which conditionally expresses Braf kinase (Braf^{V600E}) mutation and PTEN deletion, to determine whether rosiglitazone sensitizes non-T cell-inflamed melanoma to anti-PD-1 monoclonal antibody[9,29,31]. We found that anti-PD-1 mAb failed

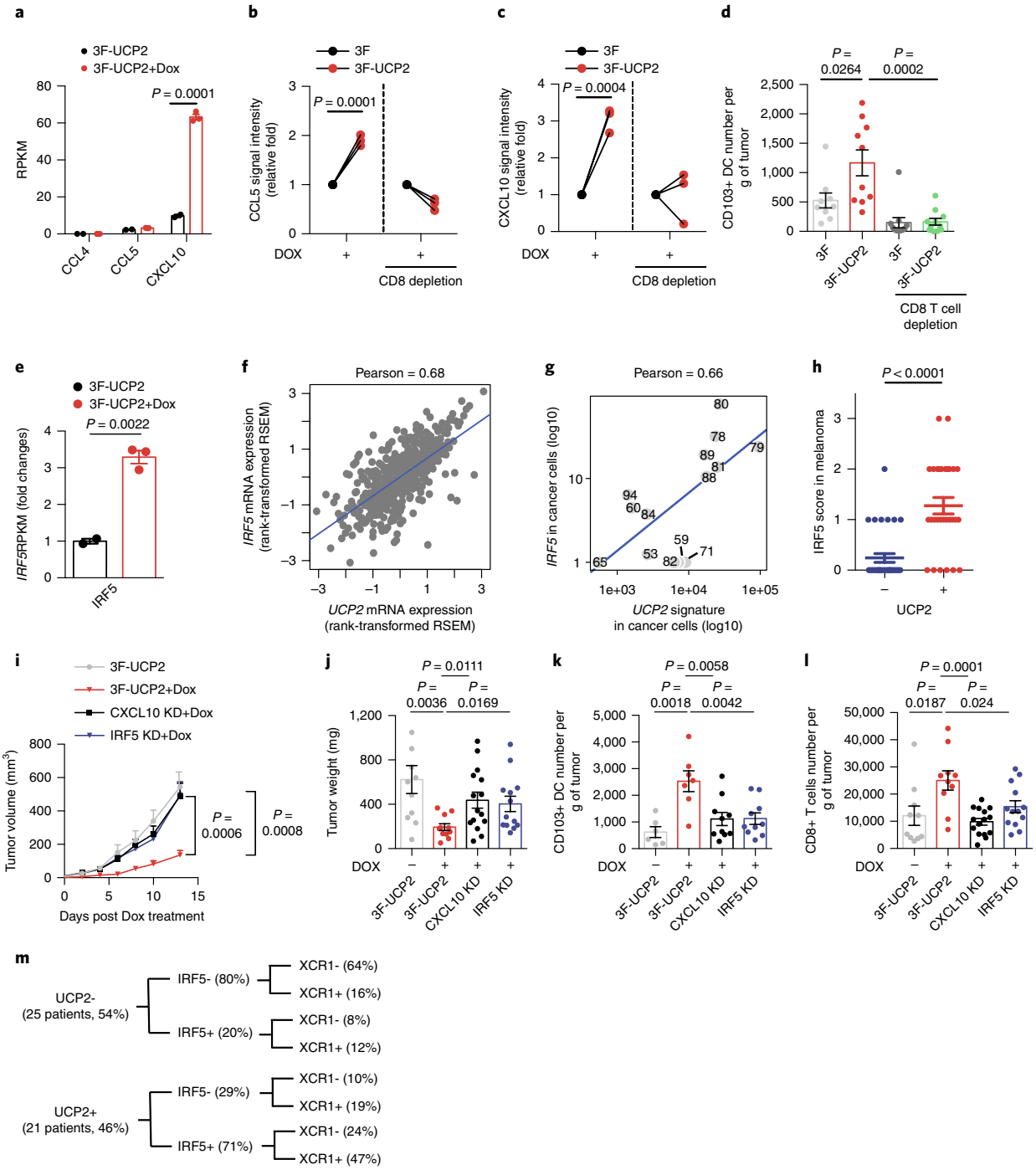

Fig. 5 | UCP2-stimulated IRF5-CXCL10 axis supports engagement of the cDC1-CD8+ T cell anti-tumor cycle. a, Expression of genes encoding indicated chemokines in 3F-UCP2 B16-OVA melanoma cells treated with control vehicle or Dox in vitro for 3 days (RPKM, reads per kilobase million) (3F-UCP2, $n=2$; 3F-UCP2 + Dox, $n=3$). **b**–**d**, Quantitative results for CCL5 (**b**) and CXCL10 (**c**) protein levels from proteomic array analysis and absolute number of CD103$^+$ dendritic cells (DCs) per gram tumor (**d**) in 3F and 3F-UCP2 B16-OVA melanomas from co-engrafted mice treated with Dox with or without CD8 T cell-depleting antibody. (**b**,**c**, each group, $n=3$; **d**, 3F, $n=9$; 3F-UCP2, $n=10$; CD8 depletion 3F, $n=11$; CD8 depletion 3F-UCP2, $n=11$). **e**, Expression of *IRF5* in 3F-UCP2 B16-OVA melanoma cells from RNA-seq analysis (3F-UCP2, $n=2$; 3F-UCP2 + Dox, $n=3$). **f**, Correlation of *UCP2* gene expression with transcript of *IRF5* in melanoma TCGA cohort. **g**, Association between the expression of UCP2 signature and IRF5 gene expression in melanoma cells of the single-cell RNA-seq dataset (Pearson correlation = 0.66, $P=0.005$, $n=14$). **h**, Quantitative results of immunohistochemistry staining against IRF5 in human melanoma sample. Sample size: UCP2$^-$ ($n=25$); UCP2$^+$ ($n=21$). **i**–**l**, Tumor growth (**i**), tumor weight (**j**), absolute number of CD103$^+$ DCs per gram tumor (**k**) and absolute number of CD8$^+$ T cells per gram tumor (**l**) of indicated melanomas from mice treated or not with Dox. CXCL10KD: CXCL10-knockdown (KD) 3F-UCP2 B16-OVA cells; IRF5KD: CCL5-KD 3F-UCP2 B16-OVA cells. (**i**,**j**, Dox$^-$ group: 3F-UCP2, $n=11$; Dox$^+$ group: 3F-UCP2, $n=11$; CXCL10 KD, $n=15$; IRF5 KD, $n=13$. **k**, Dox$^-$ group: 3F-UCP2, $n=6$; Dox$^+$ group: 3F-UCP2, $n=7$; CXCL10 KD, $n=10$; IRF5 KD, $n=10$. **l**, Dox$^-$ group: 3F-UCP2, $n=10$; Dox$^+$ group: 3F-UCP2, $n=10$; CXCL10 KD, $n=15$; IRF5 KD, $n=13$). **m**, Scheme indicating separation of 46 human melanoma patients, based on the expression of UCP2 and IRF5 in melanoma cells and XCR1 staining in tumor-infiltrating DCs. Data are mean ± s.e.m., analyzed by unpaired, two-tailed Student's *t*-test. Data are cumulative results from at least three independent experiments (**a**–**e**,**i**–**l**). Each symbol represents an individual mouse.

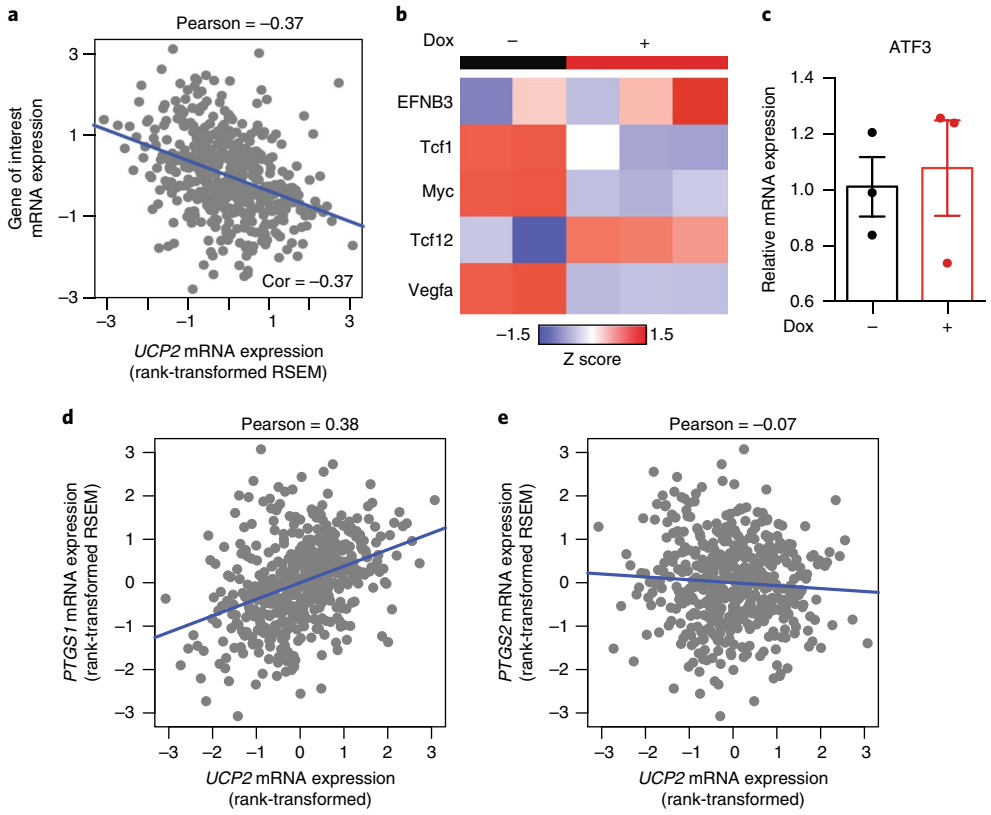

Fig. 6 | UCP2-mediated tumor suppression is independent of the β-catenin-ATF3 pathway and PGE2 production. a, Pearson correlation plots of *UCP2* expression with *CTNNB1* score in TCGA melanoma patients (Pearson correlation = 0.37, $P < 0.05$, $n = 472$, biologically independent melanoma tumor samples from TCGA cohort). **b**, Expression of indicated β-catenin pathway activated genes in 3F-UCP2 B16-OVA melanoma cells treated with control vehicle or Doxy (Dox^-, $n = 2$; Dox^+, $n = 3$). **c**, Expression of ATF3 mRNA in 3F-UCP2 B16-OVA treated or not with Dox ($n = 3$ in each group). Data are mean ± s.e.m. and were analyzed by unpaired, two-tailed Student's *t*-test. Data are a representative result from three independent experiments. **d**,**e**, Pearson correlation plots of *UCP2* expression with transcripts of *PTGS1* (Pearson correlation = 0.38, $P < 0.05$) (**d**) or *PTGS2* (Pearson correlation = 0.07) (**e**) in TCGA melanoma patients ($n = 472$, biologically independent melanoma tumor samples from TCGA cohort).

to restrict melanoma progression; however, combined treatment with anti-PD-1 monoclonal antibody and rosiglitazone stabilized tumor progression in Braf/Pten mice (Fig. 7j,k). Collectively, these findings reveal that UCP2 induction alleviates primary resistance to anti-PD-1 treatment and provides evidence of an anti-diabetic drug that could be used in cancer treatment by exploiting cDC1-dependent anti-tumor responses.

Discussion

Engagement of oncogenic pathways in tumor cells has been suggested as being a critical mechanism by which they expel $CD8^+$ T cells from the TME[11]. However, it remains challenging to trigger the anti-tumor immune cycle by alleviating the immunosuppressive features of the TME in the absence of targetable oncogenic pathways. Here we show that UCP2 expression in melanoma cells determines the immune state of the TME. UCP2 induction shifts the cytokine milieu in the TME and subsequently leads to engagement of the cDC1-$CD8^+$ T cell anti-tumor immune cycle. Moreover, enforced expression of UCP2, using either the genetic or pharmacological approach, converts the non-T-cell-inflamed TME into an immunostimulatory microenvironment that facilitates anti-tumor immunity and overcomes primary resistance to anti-PD-1 treatment. Of note, our results suggest that the regulation of UCP2 expression is independent of known oncogenic pathways, and that UCP2 expression in melanoma cells is associated with neither activity of the β-catenin pathway nor production of PGE2. Moreover, inducing UCP2 expression may represent a therapeutic strategy in initiating an anti-tumor response in those patients lacking targetable oncogenic pathways. Importantly, our results suggest that modulating UCP2 expression in melanoma cells could change the immune states of the TME, rather than systemic enhancement of immune responses, which may render the UCP2-targeting approach a broader therapeutic index for cancer treatment with less potential to induce autoimmunity.

Although we demonstrate that UCP2 induction stimulates CXCL10 production in melanoma cells in an IRF5-dependent manner, it remains unclear by which underlying mechanisms UCP2 stimulates IRF5 expression and activity. Intriguingly, expression of UCP2, but not other members of the UCP protein family, is associated with elevated T cell infiltration and formation of immune-stimulatory cytokine milieus in the TME. This implies that UCP2 may influence the immune state of the TME by its own unique functions, instead of through the mitochondrial uncoupling effect. Importantly, overexpression of UCP2 in melanoma cells fails to suppress ROS production, suggesting that the uncoupling function of UCP2 may not be engaged in melanoma cells. Some studies have suggested that increased UCP2 expression provides stress-protective signals and metabolic adaptation in response to stress insults in a variety of cells[20,44,45]. Furthermore, immune-related tissues can upregulate IRF5 expression as a result of stress response, and to support antiviral immunity[46]. It will be worthwhile to further delineate which stress responses initiated by UCP2 induction lead to upregulation of IRF5 expression and how IRF5 influences the capability of melanoma cells in immune evasion. The answers to these

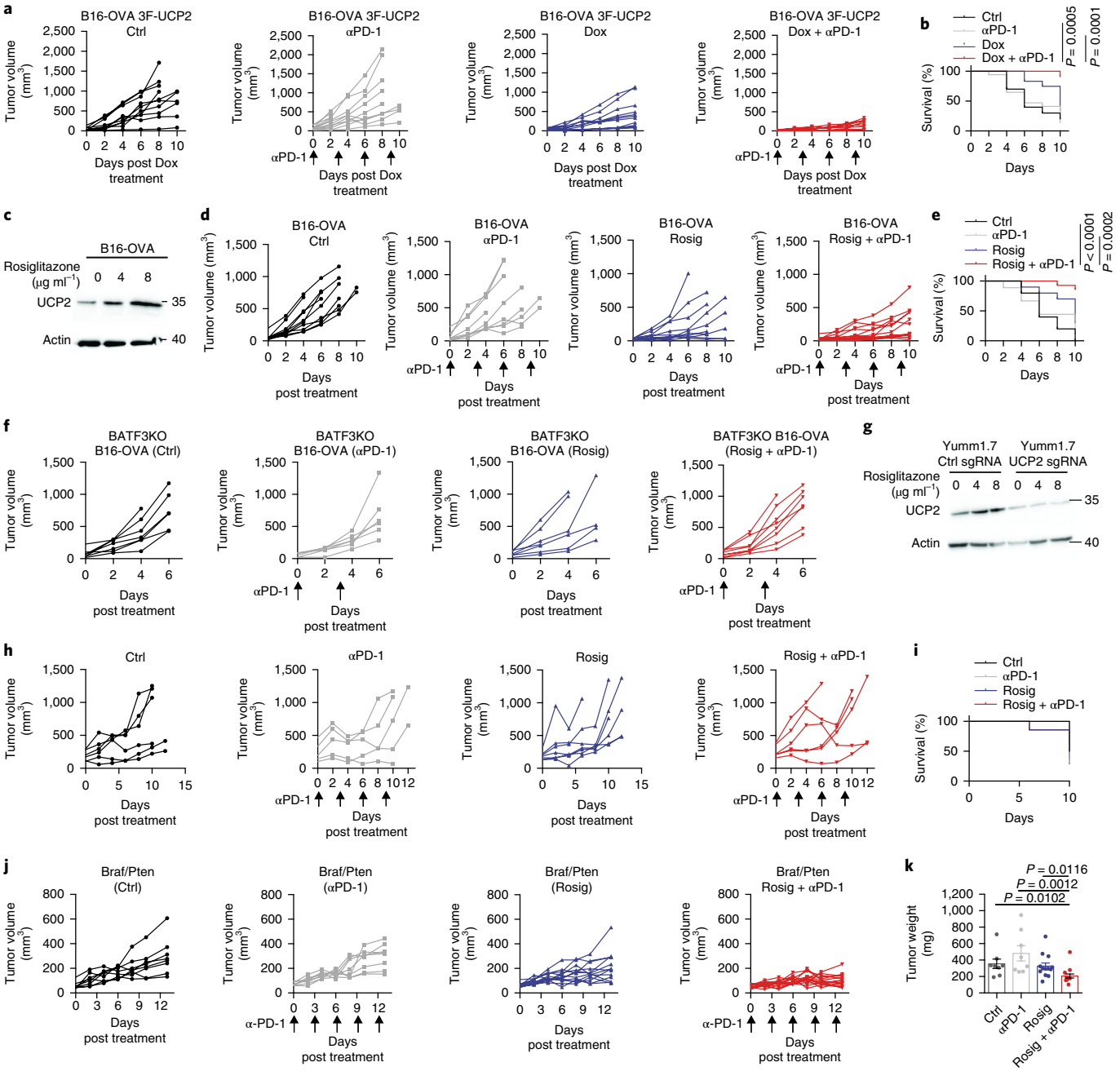

Fig. 7 | UCP2 induction sensitizes melanoma to PD-1 blockade therapy. a,**b**, Tumor growth (**a**) and Kaplan–Meier survival curves (**b**) of 3F-UCP2 B16-OVA melanoma-bearing mice treated with the indicated treatments. Ctrl, control vehicle ($n=10$); αPD-1, anti-PD-1 monoclonal antibody (mAb) ($n=12$); Dox, doxycycline ($n=12$); DOX + αPD-1, doxycycline plus anti-PD-1 mAb ($n=11$). **c**, Immunoblot analysis of indicated proteins in B16-OVA cells treated with either control vehicle or escalating doses of rosiglitazone. See also Supplementary Fig. 7b. **d**,**e**, Tumor growth (**d**) and Kaplan–Meier survival curves (**e**) of B16-OVA melanoma-bearing mice treated with indicated treatments. Ctrl ($n=8$); αPD-1 ($n=9$); Rosig, rosiglitazone ($n=10$); Rosig + αPD-1, rosiglitazone plus anti-PD-1 mAb ($n=14$). **f**, Tumor growth of *Batf3*$^{-/-}$ mice engrafted with B16-OVA melanoma receiving indicated treatments. Ctrl ($n=7$); αPD-1 ($n=6$); Rosig ($n=7$); Rosig + αPD-1 ($n=8$). **g**, Immunoblot analysis of UCP2 expression on Yumm1.7-Cas9 Ctrl-sgRNA and UCP2-sgRNA cells. See also Supplementary Fig. 7c. **h**,**i**, Tumor growth (**h**) and Kaplan–Meier survival curves (**i**) of Yumm1.7-Cas9 UCP2-sgRNA melanoma-bearing mice receiving indicated treatments. Ctrl ($n=6$); αPD-1 ($n=5$); Rosig ($n=7$); Rosig + αPD-1 ($n=6$). **j**,**k**, Tumor growth (**j**) and tumor weight (**k**) of inducible Braf/Pten melanoma-bearing mice treated with indicated treatments. Ctrl, $n=8$; αPD-1, $n=8$; Rosig, $n=13$; Rosig + αPD-1, $n=15$. Each symbol represents an individual mouse. Data are mean ± s.e.m., and were analyzed by unpaired, two-tailed Student's *t*-test (**k**). Differences in survival times were analyzed by long-rank (Mantel–Cox) test (**b**,**e**,**i**). Data are cumulative results from at least three independent experiments. Each line in the survival curve represents an individual mouse.

questions will provide a springboard for developing new therapeutic approaches that boost anti-tumor immunity by reprogramming the immunosuppressive TME.

We show that overexpressing UCP2 in melanoma cells promotes tumor vessel normalization in a T cell-independent manner and suppresses expression of vascular endothelial growth factor and

angiopoitein-2 in the TME. Given that simultaneous targeting of these two parameters is known to normalize tumor neovasculature and to enhance therapeutic responses to anti-PD-1 treatment[47], it is probable that UCP2-induced tumor vessel normalization is a result of reduced signals from these in tumors. Thus, it will be of interest to further investigate the underlying mechanisms by which UCP2 induction in melanoma cells normalizes tumor neovasculature.

Augmenting tumor infiltration of $CD8^+$ T cells is a desirable approach to alleviating primary resistance to ICB. Here we demonstrate that boosting UCP2 expression in melanoma cells reprograms chemokine profiles and initiates the anti-tumor immune cycle in the TME. Additionally, we discover that combined treatment with PD-1 blockade and UCP2 induction is therapeutically superior to treatment with either one alone in fighting against malignancy. Of note, our results suggest that UCP2 expression levels in melanoma cells may reflect the degree of tumor infiltration of $CD8^+$ T cells and cDC1. Given that the pre-existence of $CD8^+$ T cells in tumors is a predictive marker of therapeutic outcomes of ICB treatment[5], UCP2 expression in melanoma cells may represent a potent biomarker for evaluating the therapeutic responses of patients receiving PD-1 blockade therapy.

Online content

Any methods, additional references, Nature Research reporting summaries, source data, statements of data availability and associated accession codes are available at https://doi.org/10.1038/s41590-018-0290-0

Received: 15 May 2018; Accepted: 21 November 2018;
Published online: 21 January 2019

References

1. Wolchok, J. D. et al. Nivolumab plus ipilimumab in advanced melanoma. *N. Engl. J. Med.* **369**, 122–133 (2013).
2. Borghaei, H. et al. Nivolumab versus docetaxel in advanced nonsquamous non-small-cell lung cancer. *N. Engl. J. Med.* **373**, 1627–1639 (2015).
3. Ferris, R. L. et al. Nivolumab for recurrent squamous-cell carcinoma of the head and neck. *N. Engl. J. Med.* **375**, 1856–1867 (2016).
4. Sharma, P., Hu-Lieskovan, S., Wargo, J. A. & Ribas, A. Primary, adaptive, and acquired resistance to cancer immunotherapy. *Cell* **168**, 707–723 (2017).
5. Tumeh, P. C. et al. PD-1 blockade induces responses by inhibiting adaptive immune resistance. *Nature* **515**, 568–571 (2014).
6. Topalian, S. L., Drake, C. G. & Pardoll, D. M. Immune checkpoint blockade: a common denominator approach to cancer therapy. *Cancer Cell* **27**, 450–461 (2015).
7. Gajewski, T. F. The next hurdle in cancer immunotherapy: overcoming the non-T-cell-inflamed tumor microenvironment. *Semin. Oncol.* **42**, 663–671 (2015).
8. Joyce, J. A. & Fearon, D. T. T cell exclusion, immune privilege, and the tumor microenvironment. *Science* **348**, 74–80 (2015).
9. Spranger, S., Bao, R. & Gajewski, T. F. Melanoma-intrinsic beta-catenin signalling prevents anti-tumour immunity. *Nature* **523**, 231–235 (2015).
10. Bottcher, J. P. et al. NK cells stimulate recruitment of cdc1 into the tumor microenvironment promoting cancer immune control. *Cell* **172**, 1022–1037 e1014 (2018).
11. Spranger, S. & Gajewski, T. F. Impact of oncogenic pathways on evasion of antitumour immune responses. *Nat. Rev. Cancer* **18**, 139–147 (2018).
12. Fuertes, M. B. et al. Host type I IFN signals are required for antitumor CD8+ T cell responses through CD8{alpha}+ dendritic cells. *J. Exp. Med.* **208**, 2005–2016 (2011).
13. Woo, S. R. et al. STING-dependent cytosolic DNA sensing mediates innate immune recognition of immunogenic tumors. *Immunity* **41**, 830–842 (2014).
14. Horimoto, M. et al. Expression of uncoupling protein-2 in human colon cancer. *Clin. Cancer Res.* **10**, 6203–6207 (2004).
15. Pons, D. G. et al. UCP2 inhibition sensitizes breast cancer cells to therapeutic agents by increasing oxidative stress. *Free Radic. Biol. Med.* **86**, 67–77 (2015).
16. Derdak, Z. et al. The mitochondrial uncoupling protein-2 promotes chemoresistance in cancer cells. *Cancer Res.* **68**, 2813–2819 (2008).
17. Esteves, P. et al. Mitochondrial retrograde signaling mediated by UCP2 inhibits cancer cell proliferation and tumorigenesis. *Cancer Res.* **74**, 3971–3982 (2014).
18. Imai, K. et al. UCP2 expression may represent a predictive marker of neoadjuvant chemotherapy effectiveness for locally advanced uterine cervical cancer. *Oncol. Lett.* **14**, 951–957 (2017).
19. Pecqueur, C. et al. Uncoupling protein-2 controls proliferation by promoting fatty acid oxidation and limiting glycolysis-derived pyruvate utilization. *FASEB J.* **22**, 9–18 (2008).
20. Bouillaud, F. UCP2, not a physiologically relevant uncoupler but a glucose sparing switch impacting ROS production and glucose sensing. *Biochim. Biophys. Acta* **1787**, 377–383 (2009).
21. Gatza, M. L., Silva, G. O., Parker, J. S., Fan, C. & Perou, C. M. An integrated genomics approach identifies drivers of proliferation in luminal-subtype human breast cancer. *Nat. Genet.* **46**, 1051–1059 (2014).
22. Harlin, H. et al. Chemokine expression in melanoma metastases associated with CD8+ T-cell recruitment. *Cancer Res.* **69**, 3077–3085 (2009).
23. Parikh, J. R., Klinger, B., Xia, Y., Marto, J. A. & Bluthgen, N. Discovering causal signaling pathways through gene-expression patterns. *Nucleic Acids Res.* **38**, W109–W117 (2010).
24. Alexandrov, L. B. et al. Signatures of mutational processes in human cancer. *Nature* **500**, 415–421 (2013).
25. McGranahan, N. et al. Clonal neoantigens elicit T cell immunoreactivity and sensitivity to immune checkpoint blockade. *Science* **351**, 1463–1469 (2016).
26. Giannakis, M. et al. Genomic correlates of immune-cell infiltrates in colorectal carcinoma. *Cell Rep.* **17**, 1206 (2016).
27. Tirosh, I. et al. Dissecting the multicellular ecosystem of metastatic melanoma by single-cell RNA-seq. *Science* **352**, 189–196 (2016).
28. Hildner, K. et al. Batf3 deficiency reveals a critical role for CD8alpha+ dendritic cells in cytotoxic T cell immunity. *Science* **322**, 1097–1100 (2008).
29. Spranger, S., Dai, D., Horton, B. & Gajewski, T. F. Tumor-residing batf3 dendritic cells are required for effector T cell trafficking and adoptive T cell therapy. *Cancer Cell* **1**, 711–723.e4 (2017).
30. Roberts, E. W. et al. Critical role for cd103(+)/cd141(+) dendritic cells bearing ccr7 for tumor antigen trafficking and priming of T cell immunity in melanoma. *Cancer Cell* **30**, 324–336 (2016).
31. Ho, P. C. et al. Immune-based antitumor effects of BRAF inhibitors rely on signaling by CD40L and IFNgamma. *Cancer Res.* **74**, 3205–3217 (2014).
32. Dalla Pozza, E. et al. Role of mitochondrial uncoupling protein 2 in cancer cell resistance to gemcitabine. *Biochim. Biophys. Acta* **1823**, 1856–1863 (2012).
33. Kageyama, Y. et al. Leu-574 of human hif-1alpha is a molecular determinant of prolyl hydroxylation. *FASEB J.* **18**, 1028–1030 (2004).
34. Tian, L. et al. Mutual regulation of tumour vessel normalization and immunostimulatory reprogramming. *Nature* **544**, 250–254 (2017).
35. Huang, Y. et al. Improving immune-vascular crosstalk for cancer immunotherapy. *Nat. Rev. Immunol.* **18**, 195–203 (2018).
36. Algood, H. M. & Flynn, J. L. CCR5-deficient mice control *Mycobacterium tuberculosis* infection despite increased pulmonary lymphocytic infiltration. *J. Immunol.* **173**, 3287–3296 (2004).
37. Ren, J., Chen, X. & Chen, Z. J. IKKbeta is an IRF5 kinase that instigates inflammation. *Proc. Natl Acad. Sci. USA* **111**, 17438–17443 (2014).
38. Andrilenas, K. K. et al. DNA-binding landscape of IRF3, IRF5 and IRF7 dimers: implications for dimer-specific gene regulation. *Nucleic Acids Res.* **46**, 2509–2520 (2018).
39. Uccellini, L. et al. IRF5 gene polymorphisms in melanoma. *J. Transl. Med.* **10**, 170 (2012).
40. Zelenay, S. et al. Cyclooxygenase-dependent tumor growth through evasion of immunity. *Cell* **162**, 1257–1270 (2015).
41. Curran, M. A., Montalvo, W., Yagita, H. & Allison, J. P. PD-1 and CTLA-4 combination blockade expands infiltrating T cells and reduces regulatory T and myeloid cells within B16 melanoma tumors. *Proc. Natl Acad. Sci. USA* **107**, 4275–4280 (2010).
42. Bugge, A. et al. A novel intronic peroxisome proliferator-activated receptor gamma enhancer in the uncoupling protein (UCP) 3 gene as a regulator of both UCP2 and -3 expression in adipocytes. *J. Biol. Chem.* **285**, 17310–17317 (2010).
43. Villarroya, F., Iglesias, R. & Giralt, M. PPARs in the control of uncoupling proteins gene expression. *PPAR Res.* **2007**, 74364 (2007).
44. Bechmann, I. et al. Brain mitochondrial uncoupling protein 2 (UCP2): a protective stress signal in neuronal injury. *Biochem. Pharmacol.* **64**, 363–367 (2002).
45. Hass, D. T. & Barnstable, C. J. Uncoupling protein 2 in the glial response to stress: implications for neuroprotection. *Neural Regen. Res.* **11**, 1197–1200 (2016).
46. Sun, S. & Zhou, J. Molecular mechanisms underlying stress response and adaptation. *Thorac. Cancer* **9**, 218–227 (2018).
47. Schmittnaegel, M. et al. Dual angiopoietin-2 and VEGFA inhibition elicits antitumor immunity that is enhanced by PD-1 checkpoint blockade. *Sci. Transl. Med.* **9**, eaak9670 (2017).

Acknowledgements

This study was supported in part by the Swiss Institute for Experimental Cancer Research (no. ISREC 26075483), the Swiss Cancer Foundation (no. KFS-3949-08-2016), a SNSF project grant (no. 31003A_163204), a Clinic and Laboratory Integration Program

award from the Cancer Research Institute, a Harry J. Lloyd Charitable Trust Career Development Grant, a Roch-pRED grant and a SITC-MRA Young Investigator Award to P.-C.H. A.Z. and P.R. are supported by SNSF project grants (no. 320030_162575 to A.Z., nos. CRSII3_160708 and 31003A_156469 to P.R.). T.P. is supported by the MEDIC Foundation and Swiss Cancer League (no. KLS 3406-02-2016) and G.C. is supported by the Giorgi-Cavaglieri Foundation. We also thank Camilla Jandus for providing human melanoma cell lines.

Author contributions

W.-C.C. and P.-C.H. contributed to overall project design and wrote the manuscript. W.-C.C., Y.-C.T., S.R. and F.F. performed in vitro and in vivo animal experiments and data analysis. V.H.K., H.L., A.Z. and K.M. conducted the collection and immunohistochemical staining of human melanoma samples. V.H.K. and K.M. examined pathological sections. M.M. and G.C. performed computational analyses of TCGA datasets and single-cell RNA-seq. B.T., D.S. and P.R. provided essential materials and data analysis. S.R. and T.V.P. conducted and analyzed tumor blood vessel morphology and T cell infiltration.

Competing interests

W.-C.C., Y.-C.T., G.C. and P.-C.H. are inventors of patent application related to targeting of UCP2 in cancer immunotherapy. P.-C.H. received research grants from Roche and Idorsia. P.-C.H. also serves as a scientific advisory member for Elixiron Immunotherapeutics.

Additional information

Supplementary information is available for this paper at https://doi.org/10.1038/s41590-018-0290-0.

Reprints and permissions information is available at www.nature.com/reprints.

Correspondence and requests for materials should be addressed to P.-C.H.

Publisher's note: Springer Nature remains neutral with regard to jurisdictional claims in published maps and institutional affiliations.

Methods

Mice, tumor engraftment and in vivo treatment of tumor-bearing mice. C57BL/6/J, *Rag1*$^{-/-}$ (B6.129S7-Rag1^{tm1Mom}/J), *Ccr5*$^{-/-}$ (B6.129P2-Ccr5^{tm1Kuz}/J) and B6 Cas9 (B6J.129(Cg)-Gt(ROSA)26Sor$^{tm1.1(CAG-cas9*,-EGFP)Fezh}$/J) mice were purchased from Jackson Laboratory. Batf3-deficient mice (*Batf3*$^{-/-}$)[28] and Flt3L-Tg mice[48] were provided by Pedro Romero. *BRaf*^{CA}*; Tyr:CreER; Pten*$^{loxd-5}$ (Braf/Pten) mice are previously described[49]. All mice were housed in the animal facility of the University of Lausanne. For tumor induction, 3-week-old Braf/Pten mice were topically treated with 1 µl 4-hydroxytamoxifen (8 mg µl^{-1} in ethanol) on the skin surface. For tumor engraftment, tumor cell lines were injected (1×10^5 cells) subcutaneously into mice either as a single engraftment or co-engraftment as indicated in each experiment. The mice were treated with Dox-containing water (2 mg ml^{-1} Dox with 5% sucrose) on day 7 or 10 after tumor engraftment, and changed every 2 days to maintain the potency of Dox. The tumors were collected and analysis performed on day 20. For the CD8-depletion experiment, mice were treated with anti-CD8 antibody (200 µg per injection, BioXcell, clone 2.43) twice weekly during the course of experiments. For in vivo treatment, B16-OVA-bearing mice were administrated either rosiglitazone (15 mg kg^{-1}, intra-tumorally, every 2 days, Sigma-Aldrich) or control vehicle (dimethylsulfoxide), anti-PD-1 antibody (200 µg per injection, intraperitoneally, every 3 days, BioXcell, clone 29F.1A12) from day 10 post-tumor engraftment. In the Braf/Pten mouse model, four weeks after tumor induction, tumor-bearing Braf/Pten mice were treated with rosiglitazone and/or anti-PD-1 antibody as indicated above for a further 10 days. For the YUMM1.7 UCP2 single guide RNA tumor growth experiment, B6 Cas9 mice were engrafted with 1×10^6 UCP2-deficient YUMM1.7 cells. After 10 days, mice were treated as described above. For the CD8$^+$ DC and OT-I T cell co-transfer experiment, *Batf3*$^{-/-}$ mice were engrafted with 1×10^5 B16-OVA 3F-UCP2 cells. After 4 days of tumor injections, mice were treated with either control vehicle or Dox. Mice were transferred with 1×10^6 CD8$^+$ DC and 1×10^6 OT-I T cells at days 9 and 12 post-tumor engraftment, respectively. Tumor samples were collected for flow cytometry analysis at day 14. All experiments were conducted according to Swiss federal regulations, and procedures were approved by the veterinary authority of Canton Vaud.

Cell lines, plasmids, lentivirus production and transduction. The YUMM1.7 melanoma cell line was provided by Marcus Bosenberg as described previously[31,50]. The B16-OVA mouse melanoma cell line was provided by Pedro Romero. Flag tag- and flag tag-UCP2 B16-OVA or YUMM1.7 melanoma cell lines were established by stably transduced parental cell lines with lentivirus harboring Dox-inducible cassettes of indicated protein and selected by puromycin (InvivoGen). The B16-OVA cell line containing dual-inducible expression cassettes of flag tag-UCP2; HIF-1α-myc was generated by transducing the flag tag-UCP2 B16-OVA cell line with lentivirus expressing HIF-1α-myc and selected by G418. The CXCL10KD and CCL5KD melanoma cell lines were established by stably transducing flag tag-UCP2 B16-OVA with lentivirus harboring a short-hairpin RNA-expressing cassette (SMARTvector Mouse Lentiviral vector, Dharmacon), and enriched by sorting with GFP-positive populations. The YUMM1.7 Cas9 cell line were derived from YUMM1.7 transduced with pCW-Cas9, in which Dox can induce Cas9 expression. Yumm1.7-Cas9 ctrl single-guide RNA (sgRNA) (and Yumm1.7-Cas9 UCP2 sgRNA was established by stably transducing Yumm1.7-Cas9 cells with lentivirus harboring scramble sgRNA or UCP2 sgRNA. All cell lines were maintained in high-glucose-supplemented Dulbecco's modified Eagle's medium (DMEM, Life Technologies) with 10% fetal bovine serum (Gibco) and 100 U ml^{-1} penicillin-streptomycin (Thermo Fisher Scientific). For flag tag and flag tag-UCP2 melanoma cell lines, cells were maintained in culture media containing puromycin. The flag tag-UCP2 HIF-1α-myc melanoma cell line was maintained in the presence of puromycin plus blasticidin.

Doxycycline-inducible protein expression plasmids were all created in the pCW-Cas9 backbone (Addgene no. 50661). The murine UCP2 coding sequences were amplified by PCR and then cloned into pCW-Cas9 by NheI and BamH1. pCW-HIF-1a-myc was created in two steps. We first replaced the selection marker of pCW-Cas9 with blasticidin-resistant genes generated from pLX-sgRNA (Addgene no. 50662). The HIF-1α-myc-encoding sequence was amplified from pcDNA3 mHIF-1α MYC (P402A/P577A/N813A) (Addgene no. 44028) by PCR and then cloned into a pCW-Blast vector with NheI and AgeI. The lentiviral vectors harboring shRNAi against CXCL10 and CCL5 were purchased from Dharmacon (SMARTvector, V3SM11241 and V3SM11244). Lentivirus was produced by transfecting 293T cells with the indicated expression plasmids and packing these using TurboFect (Thermo Fisher Scientific). For lentiviral transduction, cells were incubated with medium containing virus and 8 µg ml^{-1} polybrene for 24 h. Cells were allowed to recover for 48 h before antibiotic selection. Detailed information on cell lines can be found in the Life Sciences Reporting Summary.

Primary immune cell isolation and in vivo injection. OT-I T cells were isolated from splenocytes of OT-I mice and cultured in Roswell Park Memorial Institute (RPMI) medium with 10% fetal bovine serum, 1% penicillin-streptomycin and β-mercaptoethanol. To activate OT-I cells, OT-I splenocytes were treated with 1 µg ml^{-1} OVA257-264, 1 µg ml^{-1} anti-CD28 and 10 ng ml^{-1} IL-2 for 3 days, then cultured in the presence of IL-2 for another 2 days before adoptive transfer or in vitro effector:target cell assay. B6 mice received 50 µl of serum from Flt3L mice daily to enrich the CD8$^+$ DC population. After 9 days of treatment, CD11c$^+$ DCs were isolated from the spleen using EasySep™ Release Mouse Biotin Positive Selection Kit (STEMCELL) and anti-CD11c Biotin (N418, Biolegend). Isolated CD11c$^+$ dendritic cells were activated with 5 mg ml^{-1} poly(I:C) (InvivoGen) for 24 h, then stimulated with 1 µg ml^{-1} OVA257-264. For each dendritic cell preparation, activation marker expression was analyzed by flow cytometry with the majority of cells being CD11c$^+$. After activation, cells showing high expression of MHCI and MHCII molecules were observed. Injection of CD8$^+$ dendritic cells was based on the percentage of CD8 expression on CD11c$^+$ DC; each mouse was administered 1×10^6 CD8$^+$CD11c$^+$ DCs intravenously.

TCGA data collection and analysis. Gene expression data for more than 10,000 cancer samples profiled by TCGA were collected from the FireHose data repository (https://gdac.broadinstitute.org/). Clinical data were also retrieved from the same source. The T cell infiltration gene expression signature was previously defined[9]. The gene signature includes the following 13 genes: CD8A, CCL2, CCL3, CCL4, CXCL9, CXCL10, ICOS, GZMK, IRF1, HLA-DMA, HLA-DMB, HLA-DOA, HLA-DOB. We used the single-sample Gene Set Enrichment analysis algorithm[51], implemented in R package GSVA, to calculate a T cell infiltration signature score for each sample. Default parameters from the GSVA package were used. Spearman correlation was used to quantify the association between UCP2 gene expression and T cell infiltration score, individually for each tumor type. The association between UCP2 expression and survival was evaluated by Cox regression and Kaplan–Meier analysis. For the latter, samples were stratified in three groups according to their UCP2 gene expression (low, intermediate, high). The 25th and 75th percentiles were used as cutoff thresholds. Survival analysis was performed separately for each tumor type.

UCP2 signature definition and projection for single-cell RNA-seq analysis. A two-step computational methodology was developed to define the UCP2 signature in malignant cells, combining the single-cell RNA-seq profiling of 19 melanoma samples from Tirosh et al.[27] and the bulk RNA-seq data of TCGA melanoma cohort. Step 1: exploiting scRNA-Seq data, the set of genes predominantly expressed in malignant melanoma cells rather than in the other infiltrating cell types was pre-selected. Then, the average expression of each of these genes in each cell type was quantified using the measure introduced by Schelker et al.[52]. All genes whose average expression in malignant cells exceeded that in infiltrating cells by at least 0.5 were retained (393 candidate genes in total). Step 2: leveraging the sample size and statistical power of TCGA melanoma dataset, we tested whether the expression of these 393 candidate genes selected in step 1 correlated with increased levels of UCP2 expression. TCGA samples were stratified in three classes based on their UCP2 expression (UCP2^{lo}, UCP2^{mid}, UCP2^{hi}), using 550 and 2,200 (roughly the 25th and 75th quantiles of UCP2 gene expression distribution) as cutoff thresholds. Next, the differential expression of the candidate genes between UCP2^{lo} and UCP2^{hi} was tested by one-sided (right-sided) Wilcoxon rank-sum test. Genes with a nominal $P > 0.05$ were discarded, retaining 49 genes as UCP2 signature (Supplementary Table 2). UCP2 signature was projected on the datasets of Tirosh et al.[27], using this as a representative proxy of UCP2 expression in melanoma cells. In single-cell RNA-seq data, the UCP2 signature was quantified by summing the expression of all signature genes in malignant cells, thus ignoring the expression of these genes in other cell types. Melanoma samples with either no T cells or no tumoral cells were excluded from this analysis. Each dot represents a sample from the dataset (with numbers corresponding to the original sample identity from Tirosh et al.[27]).

Human patient immunohistochemistry and assessment. This study was carried out in accordance with the guidelines of the Cantonal Ethics Committee Basel, under approved protocols (nos KEK-EKBB-No. 326-12, 2016-01134 and 2016-01499). All patients included in study had a history of resected primary cutaneous melanoma. Serial sections were cut from formalin-fixed paraffin-embedded tissue blocks of melanomas. De-paraffinization was performed according to standard protocols. Sections were pretreated and stained with a polyclonal antibody directed against UCP2 (NBP1-51221, Novus Biologicals), mouse anti-human CD8 (4B11, NCL-L-CD8-4B1), rabbit anti-human PD-L1(SP263, Ventana), mouse anti-human melanin A (A103, M7196, DAKO), IRF5 mouse monoclonal antibody (ABCAM, ab33478, clone number 10T1) and rabbit polyclonal anti-XCR1 antibody (ATLAS ANTIBODIES, HPA013169) on a Leica-Bond™ III/max autostainer platform, using Leica Bond ancillary reagents and the Bond Polymer Refine Red Detection system (Leica Biosystems). All immunohistochemical stainings were evaluated and scored by an experienced board-certified pathologist, blinded to clinical outcome. A four-tiered system was used for immunohistochemistry scoring. Detailed information can be found in the Life Sciences Reporting Summary.

Tumor digestion, cell isolation and flow cytometric analysis. Tumors were minced in RPMI with 2% FBS, intravenous collagenase (0.5 mg ml^{-1}, Sigma-Aldrich) and DNase (1 µg ml^{-1}, Sigma-Aldrich) and digested at 37 °C for 45 min. The digested samples were then filtered through a 70 µm cell strainer and washed with fluorescent activated cell sorter buffer (phosphate buffered saline with 2% fetal bovine serum and 2 mM EDTA). The cell pellets were then incubated with ACK lysis buffer (Invitrogen) to lyse red blood cells. Next, viable cells in single-cell tumor suspensions were further enriched by density gradient centrifugation (800*g*, 30 min) at room temperature

with 40% and 80% percoll (GE gealthcare) and collected from the interphase of the gradient. Fluorescent activated cell sorter analyses were performed using LSRII (BD Biosciences). Data were analyzed using FlowJo. The following antibodies were used for flow cytometry: anti-CD3ε (17A2), anti-CD4 (RM4-5), anti-CD8a (53.6.7), anti-CD11b (M1/70), anti-CD11c (N418), anti-CD19 (6D5), anti-CD45 (30-F11), anti-CD103 (2E7), anti-Gr-1 (RB6-8C5), anti–MHC class II I-A^b/I-E (M5/114.15.2), anti–MHC class I (AF6-88.5.5.3), anti-FoxP3 (MF-14), anti-NK1.1 (HP-3G10), anti-IFN-γ (XMG1.2), anti-TNF-α (MP6-XT22), anti-CD274 (10F.9G2) and anti-CXCL10 (J034D6). Cell populations were identified based on the expression markers listed here. CD4 T cells: $CD45^+/CD3^+/CD4^+$; CD8 T cells: $CD45^+/CD3^+/CD8^+$; T_{reg}s: $CD45^+/CD3^+/CD4^+/FoxP3^+$; B cells: $CD45^+/CD3^-/CD19^+$; NK cells: $CD45^+/CD3^-/NK1.1^+$; $CD103^+$ DC: $CD45^+/Gr\text{-}1^-/CD11b^-/CD11c^+/MHCII^+/CD103^+$. All antibodies were purchased from Biolegend, BD Biosciences or eBioscience. For intracellular staining, cells were stimulated with phorbol 12-myristate 13-acetate (20 ng ml^{-1}) plus ionomycin (1 μg ml^{-1}) with brefeldin A (5 ng ml^{-1}) for 5 h and then stained by the intracellular cytokine staining procedure as described[53]. Detailed product information can be found in the Life Sciences Reporting Summary.

Immunoblot analysis. Cell pellets were lysed using RIPA lysis buffer (50 mM Tris-HCl, pH7.4, 2 mM EDTA, 1% NP-40, 0.5% sodium deoxycholate, 0.1% SDS, 150 mM NaCl, 50 mM NaF) containing complete™ EDTA-free Protease Inhibitor Cocktail (Sigma-Aldrich, no. 11873580001). Protein lysates were mixed with SDS–PAGE loading dye and then subjected to SDS–PAGE for immunoblotting. The following antibodies were used for immunoblots: anti-UCP2 (D1O5V) rabbit monoclonal Ab (Cell Signaling, no. 89236), anti-HIF-1α (D2U3T) rabbit monoclonal Ab (Cell Signaling, no. 14179), anti-rabbit IgG, HRP-linked antibody (Cell Signaling, no. 7074), anti-mouse IgG, HRP-linked antibody (Cell Signaling, no. 7076), anti-Phospho-Akt (Ser473) rabbit monoclonal Ab (Cell Signaling, no. 4060), anti-Phospho-Akt (Thr308) rabbit monoclonal Ab (Cell Signaling, no. 13038), anti-Akt (pan) mouse monoclonal Ab (Cell Signaling, no. 2920), anti-Phospho-S6 Ribosomal Protein (Ser235/236) rabbit monoclonal Ab (Cell Signaling, no. 4858), anti-FLAG® M2 monoclonal antibody (Sigma-Aldrich, no. F1804) and anti-β-Actin monoclonal antibody (Sigma-Aldrich, no. A2228). Further information on antibodies used can be found in the Life Sciences Reporting Summary.

Murine tumor collection, immunofluorescent staining, image acquisition and quantifications. Tumor samples were fixed in 4% paraformaldehyde (PFA) and embedded in either paraffin or optimal cutting temperature compound; sections were stained using goat anti-mouse VE-cadherin (R&D AF1002), mouse anti-mouse SMA-Cy3 (Sigma C6198), rat anti-mouse CD8a (Invitrogen 4SM16 for paraffin sections) or rat anti-mouse CD8a (eBioscience 14-0081, for frozen sections), rabbit anti-mouse CD31 (Abcam ab28364) and goat anti-mouse VCAM-1 (R&D AF643) primary antibodies and corresponding donkey secondary antibodies conjugated with Alexa 488, 555 and 647 fluorophores (Invitrogen). Sections were mounted in Fluoromount G mounting medium supplemented with DAPI (Invitrogen).

A single section of each entire YUMM1.7 tumor from WT, *Rag1*$^{-/-}$ or WT mice treated with anti-CD8 monoclonal antibody was fully acquired using a Zeiss Axioscan. Images of B16-OVA tumors were acquired using a Zeiss LSM 880 with Airyscan confocal microscope. All data were analyzed using ImageJ software (NIH) and are presented as scatterplots, where each dot represent a single tumor calculated as the mean of entire tumor scans (Yumm1.7) or three representative images (B16-OVA). In regard to YUMM1.7 tumors, $CD8^+$ T cell infiltration, VE-$cadherin^+$ vessel density and area calculations were all automated using particle analysis and area measurements from each image in batches. Regarding B16-OVA $CD8a^+$ tumors, cell infiltration and vessel density were analyzed based on manually selected tumor margins and cores. Tumor-infiltrating $CD8a^+$ cells were quantified using particle analysis; eight random vessels per image were analyzed to quantify vessel length and diameter. Individual vessel surface area was calculated by multiplying average vessel length and width from each image. Mural cell co-localization with blood vessels was calculated by measuring the SMA intensity overlap over VE-cadherin (Yumm1.7) or CD31 (B16-OVA) masks ±2 pixels, and normalized by the mask size itself. All data are presented as fold change relative to the corresponding controls. The density of $VCAM\text{-}1^+$ and SMA^+ vessels was quantified using the Cell Counter plug-in (ImageJ), and the data are presented as percentage of total number of $CD31^+$ vessels.

RNA purification, RT-PCR, quantitative PCR, RNA sequencing and bioinformatics analysis. Cells were scraped in phosphate buffered saline with a scraper and centrifuged for 5 min at 1,500 rpm to form cell pellets. RNAs were then isolated using TRIzol reagent (Life Technologies). Complementary DNA was converted from RNA using M-MLV Reverse Transcriptase (Promega). Indicated mRNA expression was performed in triplicate by quantitative real-time RT-PCR on a LightCycler 480 Instrument II machine (Roche Life Science) using KAPA SYBR FAST qPCR Kit Master Mix (KAPA Biosystems). Relative expression was normalized by the expression of β-actin in each sample. The following primer pairs were used in this study. β-actin forward primer: 5′-TCCATCATGAAGTGTGACGT-3′; β-actin reverse primer: 5′-TACTCCTGCTTGCTGATCCAC-3′; IRF5 forward primer: 5′-GGAAGAAATGAAGCCAGCAG-3′; IRF5 reverse primer: 5′-ACCCTGGGGTAATTGGACTC-3′. For RNA sequencing, samples were collected after 3 days of treatment with Dox. DNA-free RNAs were extracted with Trizol and RNeasy Mini Kit (Qiagen). Messenger RNAs were then isolated for library construction. Libraries were sequenced on an Illumina HISEQ 2500 (Illumina). Mappable reads were analyzed using the DESeq2 package.

In vitro chemokine measurement and proteome mouse profiler cytokine array. Chemokine expression levels in the culture supernatants were measured using the LEGENDplex™ mouse proinflammatory chemokine assay kit (BioLegend). This assay was used to quantify the concentration of chemokines secreted by tumor cells, according to the manufacturer's instructions. The results were further normalized with protein concentration of tumor cell lysates in the same experiment. For proteome cytokine array, tumor samples were frozen on dry ice immediately following resection from tumor-bearing mice. Tumor samples were then resuspended in phosphate buffered saline containing protease inhibitors and 1% Triton X-100 for three cycles of freezing and thawing. From each sample, 200 μg of protein lysate was applied to each membrane of the Proteome Profiler Mouse XL Cytokine Array (R&D, ARY028). Staining and exposure were performed according to the manufacturer's instructions. The signal intensities of indicated cytokines were calculated by ImageStudio (LI-COR Biosciences).

In vitro T cellcancer cell coupling assay. The in vitro T cell–cancer cell coupling assay was performed as previously described[54]. Briefly, B16-OVA 3F or B1A 3F-UCP2 cells were treated with either control vehicle or Dox for 3 days and were then collected and resuspended in phosphate buffered saline. Next, tumor cells were labeled with carboxyfluorescein succinimidyl ester (CFSE, 5 μM, Thermo Fisher Scientific) for 30 min at 37 °C. After washing, labeled tumor cells were co-cultured with OT-I T cells in a 1:1 ratio at 37 °C. After 30 min incubation, cells were centrifuged at 200*g* for 2 min and fixed with 2% PFA for 10 min at room temperature. Cell pellets were then stained with anti-CD8a antibody and subjected to flow cytometric analysis. The population of tumor cells recognized by OT-I T cells was determined according to double-positive CFSE and CD8a signals.

In vitro effector: Target titration assay. B16-OVA 3F or B1A 3F-UCP2 cells were treated with either control vehicle or Dox for 3 days, then collected and resuspended in phosphate buffered saline as target cells. Cancer cells were treated with 5 μM CFSE. B16 cells were used as non-target cells and labeled with 0.5 μM CFSE. OT-I cells were co-cultured with treated cancer cells at various ratios (OT-I T:tumor cells, 0:1, 0.5:1, 1:1, 2:1, 5:1, 10:1, 20:1). After 5 h, tumor cell viability was examined by CFSE for FACS analysis. Cell survival percentage = 100 × (sample % target cell ÷ sample % non-target cell) ÷ (control % target ÷ control % non-target cell).

Statistical analysis. Data points represent biological replicates and are shown as mean ± s.e.m. Statistical significance was determined as indicated in the figure legends. Two-way ANOVA with Tukey's multiple comparison test was applied to determine statistical differences between different mouse models and groups for YUMM1.7 tumor immunohistochemistry staining; one-way ANOVA with Tukey's multiple comparison test was applied between B16 groups. Linear regression was applied in correlation dot plots to verify the statistical power of the data against tumor heterogeneity. Correlation analyses were performed using single-tailed Pearson correlation. False-discovery rate multiple hypothesis was used for RNA-seq analysis. Other data were analyzed using two-tailed, unpaired, Student's *t*-test. Log-rank (Mantel–Cox) test was used for survival analysis.

Reporting Summary. Further information on research design is available in the Nature Research Reporting Summary linked to this article.

Data availability

All other relevant data are available from the corresponding author on request.

References

48. Tsapogas, P. et al. In vivo evidence for an instructive role of fms-like tyrosine kinase-3 (FLT3) ligand in hematopoietic development. *Haematologica* **99**, 638–646 (2014).
49. Dankort, D. et al. Braf(V600E) cooperates with Pten loss to induce metastatic melanoma. *Nat. Genet.* **41**, 544–552 (2009).
50. Meeth, K., Wang, J. X., Micevic, G., Damsky, W. & Bosenberg, M. W. The YUMM lines: a series of congenic mouse melanoma cell lines with defined genetic alterations. *Pigment Cell Melanoma Res.* **29**, 590–597 (2016).
51. Barbie, D. A. et al. Systematic RNA interference reveals that oncogenic KRAS-driven cancers require TBK1. *Nature* **462**, 108–112 (2009).
52. Schelker, M. et al. Estimation of immune cell content in tumour tissue using single-cell RNA-seq data. *Nat. Commun.* **8**, 2032 (2017).
53. Ho, P. C. et al. Phosphoenolpyruvate is a metabolic checkpoint of anti-tumor T cell responses. *Cell* **162**, 1217–1228 (2015).
54. Gerard, A. et al. Secondary T cell-T cell synaptic interactions drive the differentiation of protective CD8+ T cells. *Nat. Immunol.* **14**, 356–363 (2013).

nature research

Corresponding author(s): NI-A26203C

Reporting Summary

Nature Research wishes to improve the reproducibility of the work that we publish. This form provides structure for consistency and transparency in reporting. For further information on Nature Research policies, see Authors & Referees and the Editorial Policy Checklist.

Statistical parameters

When statistical analyses are reported, confirm that the following items are present in the relevant location (e.g. figure legend, table legend, main text, or Methods section).

n/a	Confirmed	
☐	☒	The exact sample size (*n*) for each experimental group/condition, given as a discrete number and unit of measurement
☐	☒	An indication of whether measurements were taken from distinct samples or whether the same sample was measured repeatedly
☐	☒	The statistical test(s) used AND whether they are one- or two-sided *Only common tests should be described solely by name; describe more complex techniques in the Methods section.*
☒	☐	A description of all covariates tested
☐	☒	A description of any assumptions or corrections, such as tests of normality and adjustment for multiple comparisons
☐	☒	A full description of the statistics including central tendency (e.g. means) or other basic estimates (e.g. regression coefficient) AND variation (e.g. standard deviation) or associated estimates of uncertainty (e.g. confidence intervals)
☐	☒	For null hypothesis testing, the test statistic (e.g. *F*, *t*, *r*) with confidence intervals, effect sizes, degrees of freedom and *P* value noted *Give P values as exact values whenever suitable.*
☒	☐	For Bayesian analysis, information on the choice of priors and Markov chain Monte Carlo settings
☒	☐	For hierarchical and complex designs, identification of the appropriate level for tests and full reporting of outcomes
☒	☐	Estimates of effect sizes (e.g. Cohen's *d*, Pearson's *r*), indicating how they were calculated
☐	☒	Clearly defined error bars *State explicitly what error bars represent (e.g. SD, SE, CI)*

Our web collection on statistics for biologists may be useful.

Software and code

Policy information about availability of computer code

Data collection

Gene expression data for more than 10'000 cancer samples profiled by the Cancer Genome Atlas (TCGA) was collected from the FireHose (https://gdac.broadinstitute.org/) data repository. Clinical data were also retrieved from the same source. The T cell infiltration gene expression signature was defined before9. The gene signature consists in the following 13 genes: CD8A, CCL2, CCL3, CCL4, CXCL9, CXCL10, ICOS, GZMK, IRF1, HLA-DMA, HLA-DMB, HLA-DOA, HLA-DOB. We made use of the single sample Gene Set Enrichment analysis (ssGSEA) algorithm, and implemented in the R package GSVA, to calculate a T cell infiltration signature score for each sample. The default parameters from the GSVA package were used. Spearman correlation was used to quantify the association between UCP2 gene expression and T cell infiltration score, separately on each tumor type. The association between UCP2 expression and survival was evaluated by Cox regression and by Kaplan-Meier analysis. Human single cell RNA-seq data of 19 melanoma samples were from Tirosh et al.

Data analysis	Data points represent biological replicates and are shown as the mean ± s.e.m. Statistical significance was determined as indicated in the figure legends. Two-way ANOVA with Tukey's Multiple Comparison test was applied to determine the statistical differences between different mice models and groups in YUMM1.7 tumor immunohistochemistry staining; One-way ANOVA with Tukey's Multiple Comparison test was applied between B16 groups. Linear regression was applied in correlation dot plot to verify the statistical power of the data against tumor heterogeneity. Correlation analyses were performed using single tail Pearson correlation. FDR multiple hypothesis was used for RNA-seq analysis. Other data were analyzed two-tailed, unpaired, Student's t-test. Log-rank (Mantel-Cox) test was used for survival analysis. Significance is shown as *p < 0.05, **p < 0.01, ***p < 0.001 as described in each figure legend for ANOVA analysis. The exact p value were also indicated on the figure or figure legend.

For manuscripts utilizing custom algorithms or software that are central to the research but not yet described in published literature, software must be made available to editors/reviewers upon request. We strongly encourage code deposition in a community repository (e.g. GitHub). See the Nature Research guidelines for submitting code & software for further information.

Data

Policy information about availability of data

All manuscripts must include a data availability statement. This statement should provide the following information, where applicable:

- Accession codes, unique identifiers, or web links for publicly available datasets
- A list of figures that have associated raw data
- A description of any restrictions on data availability

t'he data that support the findings of this study are available from the corresponding author upon reasonable request.

Field-specific reporting

Please select the best fit for your research. If you are not sure, read the appropriate sections before making your selection.

☒ Life sciences ☐ Behavioural & social sciences ☐ Ecological, evolutionary & environmental sciences

For a reference copy of the document with all sections, see nature.com/authors/policies/ReportingSummary-flat.pdf

Life sciences study design

All studies must disclose on these points even when the disclosure is negative.

Sample size	No statistical methods were used to predetermine sample size. For in vivo animal experiment, each group contained at least 5 individual mice. For human study, 472 melamona patients form TCGA database were used for TCGA analysis. 19 melanoma patients from Torish. et. al were used for scRNA-seq analysis. Tissue blocks of 66 melanoma patients were used for human IHC staining.
Data exclusions	No data exclusions
Replication	All experimental findings were reliably reproduced. In many instances, the experiments have been pooled.
Randomization	Animals were randomly assigned to different treatment groups.
Blinding	Investigators performed, acquired and analyzed experiments and as such were not blinded.

Reporting for specific materials, systems and methods

Materials & experimental systems

n/a	Involved in the study
☒	☐ Unique biological materials
☐	☒ Antibodies
☐	☒ Eukaryotic cell lines
☒	☐ Palaeontology
☐	☒ Animals and other organisms
☐	☒ Human research participants

Methods

n/a	Involved in the study
☒	☐ ChIP-seq
☐	☒ Flow cytometry
☒	☐ MRI-based neuroimaging

Antibodies

Antibodies used

The following antibodies were used for flow cytometry: anti-CD3ε (17A2, Biolegend, 100217), anti-CD4 (RM4-5, Biolegend, 100545), anti-CD8a (53.6.7, Biolegend,100747), anti-CD11b (M1/70, ebioscience, 47-0112-80), anti-CD11c (N418, ebioscience, 17-0114-81), anti-CD19 (6D5, Biolegend, 115529), anti-CD45 (30-F11, ebioscience, 103125), anti-CD103 (2E7, ebioscience, 12-1031-81), anti-Gr-1 (RB6-8C5, ebioscience, 25-5931-81), anti–MHC class II I-Ab/I-E (M5/114.15.2, Biolegend,107605), anti–MHC class I (AF6-88.5.5.3, ebioscience, 12-5958-80), anti-FoxP3 (MF-14, Biolegend,126409), anti-NK1.1 (HP-3G10, ebioscience, 45-1619-41), anti-IFN-r (XMG1.2, Biolegend, 505825), anti-TNF-a (MP6-XT22, Biolegend, 506303), anti-CD274 (10F.9G2, Biolegend, 124307), anti-CXCL10 (J034D6, Biolegend, 519503).
The following antibodies were used for immunoblots: anti-UCP2 (D1O5V) rabbit monoclonal Ab (Cell signaling, #89236), anti-HIF-1α (D2U3T) rabbit monoclonal Ab (Cell signaling, #14179), anti-rabbit IgG, HRP-linked antibody (Cell signaling, #7074), anti-mouse IgG, HRP-linked antibody (Cell signaling, #7076), anti-Phospho-Akt (Ser473) rabbit monoclonal Ab (Cell signaling, #4060), anti-Phospho-Akt (Thr308) rabbit monoclonal Ab (Cell signaling, #13038), anti-Akt (pan) mouse monoclonal Ab (Cell signaling, #2920), anti-Phospho-S6 Ribosomal Protein (Ser235/236) rabbit monoclonal Ab (Cell signaling, #4858), anti-FLAG® M2 monoclonal antibody (Sigma-Aldrich, #F1804), anti-β-Actin monoclonal antibody (Sigma-Aldrich, #A2228), anti-UCP2 rabbit (D1O5V) mAb (Cell signaling, #89326).
The following antibodies were used for murine IHC: VE-Cadherin (R&D AF1002), mouse anti-mouse SMA-Cy3 (Sigma-Aldrich C6198), rat anti-mouse CD8a (Invitrogen 4SM16 for paraffin sections), rat anti-mouse CD8a (eBioscience 14-0081, for frozen sections), rabbit anti-mouse CD31 (Abcam, ab28364) and goat anti-mouse VCAM-1 (R&D AF643) primary antibodies and corresponding donkey secondary antibodies conjugated to Alexa 488, 555 and 647 fluorophores (Invitrogen). Sections were mounted in Fluoromount G mounting medium supplemented with DAPI (Invitrogen).
The following antibodies were used for human IHC: polyclonal antibody directed against UCP2 (dilution 1:100, NBP1-51221, Novus Biologicals). For PD-L1 imunohistochemistry (IHC), a rabbit monoclonal ready-to-use antibody assay (SP263, Ventana, Tucson, AZ). Mouse-anti-human CD8 (4B11, NCL-L-CD8-4B1, dilution 1:40, Novocastra, Leica Biosystems, Newcastle, UK; Bond Polymer Refine Detection = brown signal). Mouse-anti-human melan A (A103, M7196, dilution 1:200, DAKO, Glostrup, Denmark; Bond Polymer Refine Red Detection = red signal), Anti-IRF5 mouse mAb (Abcam, 10T1, ab33478, dilution 1:1600), Anti-XCR1 Rabbit polyclonal antibody (ATLAS ANTIBODIES, HPA013169, dilution 1:50).
The following antibodies were used for in vivo study: anti-CD8 antibody (200 µg per injection, BioXcell, clone 2.43), anti-PD-1 antibody (200 µg per injection, intraperitoneal injection, every three days, BioXcell, clone 29F.1A12)

Validation

Human antibodies: Validated by manufacturer using human PBMCs
Mouse antibodies: Validated by manufacturer using C57BL/6 splenocytes

Eukaryotic cell lines

Policy information about cell lines

Cell line source(s)

The original cell line YUMM1.7 melanoma cell line were provided by Marcus Bosenberg, and B16-OVA mouse melanoma cell line was provided by Pedro Romero.

Authentication

None of the cell lines were authenticated in these studies, but low passage number cell lines were utilized.

Mycoplasma contamination

All the cell lines are mycoplasma-free. They have been tested for mycoplasma contamination regularly.

Commonly misidentified lines
(See ICLAC register)

No commonly misidentified cell lines were used.

Animals and other organisms

Policy information about studies involving animals; ARRIVE guidelines recommended for reporting animal research

Laboratory animals

The strains and source of mice:
C57BL/6J (WT), Rag 1-/- (B6.129S7-Rag1tm1Mom/J), Ccr5-/- (B6.129P2-Ccr5tm1Kuz/J), B6 Cas9 (B6J.129(Cg)-Gt(ROSA)26Sortm1.1(CAG-cas9*,-EGFP)Fezh/J) : purchased form the Jackson Laboratory, and inbred in conventional animal facility in University of Lausanne.
BATF3-deficient (Batf3–/–), Flt3L-Tg: obtained form Petro Romero's lab, which originally purchased form the Jackson Laboratory.
BRafCA; Tyr::CreER; Ptenlox4-5 (Braf/Pten): obtained form Marcus Bonsenburg, Yale University, , and inbred in conventional animal facility in University of Lausanne.
Mice were 4-6 weeks old at the start of the experiments, both male mice were used.

Wild animals

No wild animals were involved

Field-collected samples

No samples were collected from the field

Human research participants

Policy information about studies involving human research participants

Population characteristics

Patient samples used in this study were collected from metastatic melanoma patients. The sample size was determined by the availability of specimens and samples used in this study were collected prior to any immune checkpoint blockade treatment or

	immunotherapy
Recruitment	Melanoma patients were consented for tumor sample collection under IRB approved protocols (EKNZ BASEC 2016-01499, EK 326/12 and EK 128/13).

Flow Cytometry

Plots

Confirm that:

☒ The axis labels state the marker and fluorochrome used (e.g. CD4-FITC).

☒ The axis scales are clearly visible. Include numbers along axes only for bottom left plot of group (a 'group' is an analysis of identical markers).

☒ All plots are contour plots with outliers or pseudocolor plots.

☒ A numerical value for number of cells or percentage (with statistics) is provided.

Methodology

Sample preparation	Tumors were minced in RPMI with 2% FBS, collagenase IV (0.5 mg/mL, Sigma-Aldrich), and DNase (1 µg/mL, Sigma-Aldrich) and digested at 37˚C for 45mins. The digested samples were then filtered through cell strainer and washed with FACS buffer (PBS with 2% FBS and 2mM EDTA). The cell pellets were then incubated with ACK lysis buffer (Invitrogen) to lyse red blood cells. Next, viable cells in tumor single cell suspensions were further enriched by density gradient centrifugation (800xg, 30min) at room temperature with 40% and 80% percoll (GE gealthcare) and collected from the interphase of the gradient.
Instrument	LSRII
Software	DIVA (BD) for data collection, FlowJo (LLC) for data analysis
Cell population abundance	N/A
Gating strategy	Cell populations were identified based on the expression markers listed below. CD4 T cells: CD45+/CD3+/CD4+; CD8 T cells: CD45+/CD3+/CD8+; Tregs: CD45+/CD3+/CD4+/FoxP3+; B cells: CD45+/CD3-/CD19+; NK cells: CD45+/CD3-/NK1.1+; CD103+ DC: CD45+/Gr-1-/CD11b-/CD11c+/MHCII+/CD103+.

☒ Tick this box to confirm that a figure exemplifying the gating strategy is provided in the Supplementary Information.